Abundance Measurements of Titan's Stratospheric HCN, HC_3N, C_3H_4, and CH_3CN from ALMA Observations

Authors: Alexander E. Thelen[a1], C. A. Nixon[b], N. J. Chanover[a], M. A. Cordiner[b,c], E. M. Molter[d], N. A. Teanby[e], P. G. J. Irwin[f], J. Serigano[g], S. B. Charnley[b]

[a]New Mexico State University, [b]NASA Goddard Space Flight Center, [c]Catholic University of America, [d]University of California, Berkeley, [e]University of Bristol, [f]University of Oxford, [g]Johns Hopkins University

Abstract

Previous investigations have employed more than 100 close observations of Titan by the *Cassini* orbiter to elucidate connections between the production and distribution of Titan's vast, organic-rich chemical inventory and its atmospheric dynamics. However, as Titan transitions into northern summer, the lack of incoming data from the *Cassini* orbiter presents a potential barrier to the continued study of seasonal changes in Titan's atmosphere. In our previous work (Thelen, A. E. et al. [2018]. Icarus 307, 380–390), we demonstrated that the Atacama Large Millimeter/submillimeter Array (ALMA) is well suited for measurements of Titan's atmosphere in the stratosphere and lower mesosphere ($\sim 100 - 500$ km) through the use of spatially resolved (beam sizes $<1''$) flux calibration observations of Titan. Here, we derive vertical abundance profiles of four of Titan's trace atmospheric species from the same 3 independent spatial regions across Titan's disk during the same epoch (2012 to 2015): HCN, HC_3N, C_3H_4, and CH_3CN. We find that Titan's minor constituents exhibit large latitudinal variations, with enhanced abundances at high latitudes compared to equatorial measurements; this includes CH_3CN, which eluded previous detection by *Cassini* in the stratosphere, and thus spatially resolved abundance measurements were unattainable. Even over the short 3-year period, vertical profiles and integrated emission maps of these molecules allow us to observe temporal changes in Titan's atmospheric circulation during northern spring. Our derived abundance profiles are comparable to contemporary measurements from *Cassini* infrared observations, and we find additional evidence for subsidence of enriched air onto Titan's south pole during this time period. Continued observations of Titan with ALMA beyond the summer solstice will enable further study of how Titan's atmospheric composition and dynamics respond to seasonal changes.

Keywords: Titan, atmosphere; Atmospheres, composition; Atmospheres, dynamics; Radio Observations; Radiative Transfer;

[1]Corresponding author. (A. E. Thelen) Email address: athelen@nmsu.edu. Postal Address: Department of Astronomy, New Mexico State University, PO BOX 30001, MSC 4500, Las Cruces, NM 88003-8001. Telephone: (831)-332-1899.

1 Introduction

Saturn's largest moon, Titan, is host to a dense, dynamic atmosphere rich with trace organic molecules produced through N_2 and CH_4 generated photochemistry. Many hydrocarbon (C_XH_Y) and nitrile ($C_XH_Y[CN]_Z$) species have been detected throughout Titan's atmosphere, often showing vertical gradients from their primary formation site in the upper atmosphere (upwards of 700 km) through N_2/CH_4 dissociation and ionospheric interactions, to condensation near the tropopause at altitudes below 80 km (see review by Hörst, 2017).

Decades after the initial discovery of Titan's atmosphere through the spectroscopic detection of CH_4 (Kuiper, 1944), additional trace hydrocarbons C_2H_2, C_2H_4, and C_2H_6 were detected through ground-based observations in the IR (Gillett et al., 1973; Gillett, 1975). N_2 and Titan's most abundant nitriles – HCN (*hydrogen cyanide*), HC_3N (*cyanoacetylene*), and C_2N_2 – were discovered through *Voyager 1* Ultraviolet Spectrometer (UVS) and Infrared Spectrometer (IRIS) observations during the spacecraft's flyby of Titan in 1980 (Broadfoot et al., 1981; Hanel et al., 1981; Kunde et al., 1981), in addition to more complex hydrocarbons such as C_3H_8 and C_3H_4 (or CH_3CCH, *methylacetylene*; Maguire et al., 1981). Many of these trace constituents were found to be enhanced at mid to high northern latitudes (>50°N, then in winter) compared to the equator and southern latitudes. In particular, the nitriles were enhanced by up to an order of magnitude near the north pole. This enrichment was initially attributed to the shielding of the winter pole from UV radiation due to Titan's obliquity of $\sim 26°$, mitigating the rapid depletion of nitriles and some hydrocarbons in the stratosphere, and potential seasonal effects (Yung, 1987; Coustenis and Bezard, 1995).

Upon the arrival of the *Cassini* orbiter to the Saturnian system in 2004 (nearly one Titanian year after the *Voyager 1* flyby), more in-depth observations of Titan's atmospheric composition and dynamics were possible through the close monitoring of the moon over 127 targeted flybys, often within 1000 km of the moon's surface and well within its ionosphere, and the deployment of the *Huygens* probe to Titan's surface in 2005. A campaign of studies investigating Titan's atmosphere revealed further complex chemistry, a wealth of unidentified heavy positive and negative ions in the upper atmosphere, additional hydrocarbons and nitriles, and confirmation that the distributions of Titan's complex chemical species are connected to its atmospheric dynamics (see reviews in Bézard et al., 2014; Vuitton et al., 2014). The enhancement of many trace chemicals above Titan's north pole was again observed during northern winter, followed by a change from south-to-north circulation to a two cell pattern with upwelling onto both poles, and finally into a completely reversed, north-to-south circulation cell in 2011 (Flasar et al., 2005; Teanby et al., 2008; Teanby et al., 2010a; Teanby et al., 2012; Vinatier et al., 2015; Coustenis et al., 2016).

The results of *Voyager 1* studies of Titan prompted the use of mm/sub-mm ground-based observations (Paubert et al., 1984), leading to the confirmation of the existence of HCN, HC_3N (Paubert et al., 1987; Bézard et al., 1992), and the detection of CH_3CN (*methyl cyanide*) (Bézard et al., 1993) with the IRAM 30-m telescope; the latter molecule appeared to be of comparable abundance to Titan's other nitriles through laboratory experiments (Raulin et al., 1982), but eluded detection in the IR during the *Voyager* and *Cassini* eras. The vertical profiles of these molecules have since been studied from the ground with IRAM (Marten et al., 2002), the Submillimeter Array (SMA; Gurwell, 2004), and most recently, the Atacama Large Millimeter/submillimeter Array (ALMA; Cordiner et al., 2014; Molter et al., 2016), which is also capable of detecting C_3H_4, HNC, C_2H_3CN, C_2H_5CN, and potentially other trace nitriles (Teanby et al., 2018; Cordiner et al., 2015; Palmer et al., 2017; Lai et al., 2017). While early mm/sub-mm studies of Titan have resulted in disk-averaged measurements of these minor constituents, ALMA currently provides the capabilities to study the spatial variation of many species through resolved observations of Titan, which is $\sim 1''$ on the sky (including its extended atmosphere) compared to the maximum resolution obtainable with ALMA of few–10s of mas. The frequent observations of Titan for ALMA flux calibration measurements facilitates the continuation of *Cassini's* legacy, allowing for studies of Titan's climate and atmospheric chemistry beyond the northern summer solstice.

Thelen et al. (2018) – hereafter referred to as 'Paper I' – showed that ALMA flux calibration observations of Titan enable the measurement of spatial variations in stratospheric temperature. While the viewing geometry and spatial resolution of early flux calibration data only permitted large latitudinal averages on three separate regions on Titan, the temperature measurements discussed in Paper I were in agreement with those found by the *Cassini* Composite Infrared Spectrometer (CIRS); however, the spatial and (in particular) temporal variations in temperature profiles were minor in these large 'beam-footprints' compared to those seen with the exceptional latitudinal resolution of *Cassini* (Achterberg et al., 2011; Vinatier et al., 2015; Coustenis et al., 2016). Here, we seek to use the methodology established in Paper I to further probe Titan's atmospheric composition and dynamics through the stratospheric measurements of HCN, HC_3N, CH_3CN, and C_3H_4. We present the first spatially-resolved abundance measurements of these species from ground-based radio observations, utilizing data from 2012 to 2015 as Titan transitioned into northern summer. We discuss the comparisons of these measurements to those from contemporary *Cassini*/CIRS observations and photochemical models, and demonstrate the potential for further studies of spatial and temporal variations in Titan's trace atmospheric species after the end of the *Cassini* mission using ALMA.

2 Observations

We utilize flux calibration data of Titan from the ALMA science archive[2], and follow the procedures in Paper I to reduce and calibrate datasets. This includes the modification of data reduction scripts provided by the Joint ALMA observatory to avoid the flagging (removal) of strong atmospheric lines from Titan's atmosphere, general imaging procedures, and the extraction of disk-averaged spectra. The observational parameters for these data are detailed in Table 1. Datasets were chosen based on spatial resolution and observation date, with preference given to the highest resolution data observed closest to the data analyzed in Thelen et al. (2018) used to obtain temperature measurements in Titan's stratosphere. The list of detected and modeled transitions for each species is listed in Table 2.

We modeled disk-averaged spectra for all datasets listed in Table 1, and spectra from three independent spatial regions for the nitrile species from either 2012 or 2013, and for all species in 2014 and 2015. While spectra representing Titan's northern and southern hemispheres were extracted for C_3H_4 in 2013, the signal-to-noise ratio was insufficient to yield meaningful abundance retrievals. As in Paper I, spatially resolved spectra were extracted from regions where ALMA 'beam-footprints' do not overlap to obtain independent measurements of three spatial regions. These regions were chosen to match those in Paper I as closely as possible – with mean latitudes at or within 3° of 48° N, 21° N, and 16° S (hereon referred to as 'North', 'Center', and 'South') – so that we may ensure corresponding temperature measurements are appropriate for chemical abundance retrievals. These regions are held constant with Titan's changing tilt from 2012 to 2015. As we do not expect to see longitudinal changes in chemical abundance, we extracted spectra representing Titan's low northern latitudes (Center) in some higher resolution data in 2014 and 2015 from Titan's limb, as opposed to Titan's central disk where emission from atmospheric species is reduced leading to insufficient fluxes. Integrated flux (moment 0) maps are shown for HC_3N and CH_3CN in Fig. 1 for 2013, 2014, and 2015, demonstrating the spatial variation of these molecules in Titan's stratosphere.

[2]https://almascience.nrao.edu/alma-data/archive

3 Spectral Modeling and Retrieval Methodology

Models of Titan's atmospheric structure and the subsequent generation of synthetic spectra were carried out in a similar fashion to Paper I. Molecular line data were obtained from the HITRAN 2016[3] and CDMS[4] catalogues (Gordon et al., 2017; Müller et al., 2005). We employed the Non-Linear Optimal Estimator for Multivariate Spectra Analysis (NEMESIS) radiative transfer code in line-by-line mode (Irwin et al., 2008) to retrieve vertical abundance profiles from 0–1200 km for each gas species independently. As in Paper I (and detailed in Teanby et al., 2013), many field-of-view averaging points (37-44) are required to model disk-averaged data, with higher concentrations of emission angles on Titan's limb. For spatially resolved spectra, field-of-view points were weighted to model emission from each ALMA beam-footprint. Spectra were multiplied by a small scaling factor found by modeling nearby regions of continuum emission to account for small offsets due to flux calibration or model inaccuracies. Using accurate troposphere temperatures from *Cassini* radio science measurements (Schinder et al., 2012, following the procedures detailed in Paper I) reduced these scaling factors to below 5% of the continuum flux, within the expected calibration uncertainty level (see ALMA Memo #594[5]). ALMA data and the resulting best fit spectra for each molecule in each year are shown in Fig. 2–5.

While chemical abundance contributes to the radiance of molecular line cores in Titan's upper atmosphere (~800 km), we only discuss the retrieval results for the upper troposphere–stratosphere (50–550 km) here, where our previous ALMA retrievals of temperature are valid (Paper I) and the rotational emission lines are not subject to non-LTE and thermal broadening effects (Yelle, 1991; Cordiner et al., 2014); additionally, the few data points that make up the line centers in these data contribute little to the χ^2 minimization of data and model discrepancies, and the retrieved abundance profiles often return to the *a priori* profile values in the upper atmosphere as in previous studies of ALMA data using NEMESIS (Serigano et al., 2016; Molter et al., 2016; Thelen et al., 2018). Contribution functions generated for disk-averaged spectra of each molecule are shown in Fig. 6, showing significant contribution between ~100–300 km (10–0.1 mbar) for each molecule, and secondary peaks in the upper atmosphere.

For all gases in this study, multiple *a priori* abundance profiles were tested to determine uniqueness amongst retrieved measurements (see example in Section 3.1). Similar to the previous temperature retrievals in Paper I, we have elected to use data besides those obtained by *Cassini*/CIRS data to generate *a priori* profiles (i.e. profiles with more simple vertical structure) where possible, to facilitate the use of ALMA for future Titan measurements after the end of the *Cassini* era. These often include previous disk-averaged observations of Titan in the sub-mm or results from photochemical models. *A priori* vertical profiles were taken with 100% errors at all altitudes and correlation lengths were set to 1.5 scale heights (as in Teanby et al., 2007) for all species but the HCN isotopologues (set to 3.0, as in Molter et al., 2016) to provide sufficient vertical smoothing, and to account for uncertainties due to minor variations in temperature, line broadening parameters, and ALMA flux calibrations. The specific parameters, *a priori* profiles, and retrieval methodology pertaining to each gas species are discussed in the following subsections.

To ensure the accurate retrieval of continuous chemical abundance profiles, we modeled emission lines without any contamination from other species where possible, and held atmospheric temperatures constant. Both spatially resolved and disk-averaged temperature profiles from Paper I were used to model 2012, 2014, and 2015 spectra, providing measurements from similar latitude regions within ~2 months of the datasets analyzed here (Table 1); temperature variations in Titan's stratosphere

[3]http://hitran.org/
[4]https://www.astro.uni-koeln.de/cdms/catalog
[5]https://science.nrao.edu/facilities/alma/aboutALMA/Technology/ALMA_Memo_Series/alma594/memo594.pdf

are negligible on these timescales (Flasar et al., 1981), particularly for measurements comprised of multiple latitudes such as those analyzed here (see Paper I). For 2013 data, we elected to use more contemporary temperature profiles obtained during the T89 and T91 *Cassini* flybys (during February 17 and May 23, respectively) obtained with the CIRS instrument (courtesy R. Achterberg, private communication; see also Achterberg et al., 2011; Achterberg et al., 2014). All temperature profiles used in this study are are shown in Fig. 7. As emission lines in Titan's atmosphere may be significantly affected by temperature variations, we tested the discrepancies found in Paper I between retrieved ALMA and *Cassini*/CIRS temperature profiles (∼0–5 K for spatial regions) on HCN isotope lines; we find that variations of temperature on order 5 K or less resulted in abundance variations $<20\%$, and were well within the retrieval errors.

3.1 HC_3N and C_3H_4

For both molecules, we assumed a Lorentzian broadening HWHM (Γ) value $= 0.1$ cm^{-1} bar^{-1} and temperature dependence (α) $= 0.75$ as in previous studies (Vinatier et al., 2007; Cordiner et al., 2014; Lai et al., 2017) and recommended by HITRAN. The strongest 4-5 C_3H_4 transitions were modeled each year, as weaker lines did not significantly contribute to the retrieved vertical abundance profiles. For the 2015 dataset, 2 interloping C_2H_5CN lines were modeled among the C_3H_4 bandhead, except in the Center spectrum, where these lines did not significantly impact the χ^2 value.

The initial HC_3N abundance profiles used as *a priori* inputs came from previous disk-averaged measurements of Titan in the sub-mm by Cordiner et al. (2014) and Marten et al. (2002). A comparison of these profiles to fractional scale height and continuous abundance retrievals is shown in Fig. 8. While adequate fits of disk-averaged lines at low S/N can be accomplished using fractional scale height ('gradient') profiles as in Cordiner et al. (2014), we find that spectral fits are improved by using continuous abundance retrievals (Fig. 8A); for all chemical species, spatial spectra are fit better by continuous retrievals due to broadened line wings (compare, e.g., HC_3N spectra in Fig. 4). Additionally, the gradients present in some continuous vertical profiles are important for the study of temporal and dynamical variations. For a variety of *a priori* profiles (Fig. 8B) or perturbations thereof, continuous retrievals converged on similar vertical profiles (Fig. 8C) for all gases modeled in this study.

Models of C_3H_4 were initialized using 'step models' of abundance, as in Cordiner et al. (2014; 2015), with a VMR $= 1 \times 10^{-8}$ at 100 km as found by Nixon et al. (2013), or by using photochemical model results from Loison et al. (2015). In 2015, additional lines of C_2H_5CN were modeled using the gradient model from Cordiner et al. (2015), comparable to that found in other ALMA studies (Palmer et al., 2017; Lai et al., 2017; Teanby et al., 2018). Spatial abundance variations of C_2H_5CN are not determined here due to the lines' proximity to those of C_3H_4 and their relatively weak strength.

3.2 HCN

Due to the strong self-absorption present in spectra of HCN from spatially resolved datasets of Titan and the calibration uncertainties for species with extensive line wings in ALMA data (as with CO, detailed in Paper I), we chose to model the HCN isotopologues $H^{13}CN$ and $HC^{15}N$ as proxies for HCN abundance. Molter et al. (2016) showed a retrieved vertical abundance profile of HCN could be scaled to fit lines of isotopologues and used to determine isotope ratios for disk-averaged spectra. Here, we reversed this process by fitting $H^{13}CN$ and $HC^{15}N$ lines using the HCN profile found by Molter et al. (2016), and applied a constant scaling factor ($^{12}C/^{13}C = 89.8$, $^{14}N/^{15}N = 72.2$) to determine the HCN abundances. As in that study, we model $H^{13}CN$ and $HC^{15}N$ lines with $\Gamma = 0.13$, $\alpha = 0.75$. We set condensation to begin at altitudes below $\sim$ 80 km as in Marten et al. (2002), which was derived from the vapor saturation law in Lellouch et al. (1994) and is consistent with the calculations based on *Cassini/Huygens* observations in Titan's lower stratosphere by Lavvas et al. (2011); below this altitude, the abundance profile no longer effects the line shape. The HCN isotope lines lie on the wings of the CO (J=3–2) and CO (J=6–5) transitions, so those lines were included in the model using the parameters given in Paper I.

While the C and N ratios found for Titan through HCN measurements have a range of values (see Molter et al., 2016 and references therein), we find that applying these ratios to line data and scaling the retrieved profiles to convert to HCN abundances have vanishingly small effects for the range of published isotope ratios. For the 2014 measurements, we were able to model both species in disk-averaged and spatially resolved spectra, and found the (scaled) retrieved profiles were in good agreement (see Section 4).

3.3 CH_3CN

For computational efficiency and to preserve the native resolution of ALMA data (i.e. without additional channel averaging to meet the array limitations of NEMESIS), we only retrieved abundance profiles using the strongest CH_3CN lines in each band. Studies of CH_3CN in Titan's atmosphere have been limited due to its lack of observable transitions in the IR accessible by *Cassini*. Therefore we tested three different *a priori* profiles and variations of those by an order of magnitude in each direction: the combination of disk-averaged measurements from Marten et al. (2002) to 500 km, and the model results from Loison et al. (2015) up to 1200 km; the model by Dobrijevic and Loison (2018), which tests a new nitrogen isotope fractionation scheme from Loison et al., 2015; a test gradient profile (Profile 1 from Fig. 8). *A priori* profiles and retrieval results are shown in Fig. 9A and B, respectively, for the 2014 disk-averaged spectrum of CH_3CN (Fig. 4). All retrievals shown in Fig. 9B provided an adequate fit to the data. We find that the retrievals converge around 150 km ($\sim$ 2 mbar) and above, where ALMA is sensitive to CH_3CN emission (Fig. 6E).

We adopted the N_2-broadening parameters detailed by Dudaryonok et al. (2015), where available. As these differ from the parameters used by Marten et al. (2002), we ran a large number of forward models of the 2014 (J=16–15) transitions to test the effect of the Lorentzian broadening and temperature dependence coefficients. Though we obtained some variation in χ^2 values for the parameter space [Γ=0.1–0.16, α=0.5–0.8] for CH_3CN forward models, the effects of these parameters on retrieved abundances were small and well within the retrieval errors for a model using the Dudaryonok et al. (2015) parameters.

4 Results and Discussion

In Fig. 10, we present the mean disk-averaged results for each molecule; the average of the scaled $HC^{15}N$ and $H^{13}CN$ profiles is used to represent HCN here. As with the temperature profiles found in Paper I, abundance retrievals from disk-averaged measurements do not show significant variation from year to year, and all fall within the retrieval errors of the mean profile. In Fig. 11–13, we present the retrieved abundance profiles from spatially resolved spectra in Fig. 2–5. HCN profiles from 2012 and HC_3N, CH_3CN profiles from 2013 are shown together in Fig. 11. Scaled HCN profiles from both $H^{13}CN$ and $HC^{15}N$ retrievals from 2014 are shown in Fig. 12. With the exception of a small portion of the Center retrievals between 0.1–1 mbar, and >10 mbar (where the HCN isotopologues quickly lose sensitivity – Fig. 6A,B), these profiles all agree and display similar vertical variations (e.g. a slight inversion in north and south retrievals at pressures <0.1 mbar).

4.1 Comparison to Previous Studies

In Fig. 14 we compare the mean disk-averaged profiles (Fig. 10) to those from previous disk-averaged sub-mm measurements of Titan and photochemical model results.

The disk-averaged HCN profile (a mean of both $H^{13}CN$ and $HC^{15}N$ profiles for all years) agrees well with previous sub-mm observations by Molter et al. (2016) with ALMA throughout the atmosphere, and with those of Marten et al. (2002) and Gurwell (2004) in the lower atmosphere. Our profile is also comparable to the photochemical models of Krasnopolsky (2014) and Dobrijevic and Loison (2018) in the stratosphere and above.

Our mean retrieved HC_3N profile shows a highly variable slope – particularly the lower atmosphere enhancement near 1 mbar – compared to both previous sub-mm observations (Marten et al., 2002; Cordiner et al., 2014) and photochemical models (Dobrijevic and Loison, 2018), though the abundance at all altitudes is significantly less than predicted by Krasnopolsky (2014). We find stratospheric abundances closest to the fractional scale height model adopted by Cordiner et al. (2014) and the models of Dobrijevic and Loison (2018). These differences may be explained by the use of continuous abundance retrievals for disk-averaged measurements, which tended towards a mean profile of the three spatial regions; HC_3N shows significant enhancement between 100–200 km in the higher northern and low southern latitudes (Fig. 11–13), which may be reflected in the disk-averaged measurements.

The mean C_3H_4 profile is consistent with previous CIRS measurements (Nixon et al., 2013), contemporary ALMA observations (Teanby et al., 2018), and photochemical models (Krasnopolsky, 2014; Loison et al., 2015) below 400 km, where ALMA is most sensitive to C_3H_4 emission (Fig. 6D).

Above 200 km, we find that our CH_3CN profile is consistent with previous sub-mm observations by Marten et al. (2002) and the photochemical model of Dobrijevic and Loison (2018), though generally less than that of Krasnopolsky (2014). We find CH_3CN to be a factor of ~ 5 less than the upper limit found by Nixon et al. (2010) at 25°S in *Cassini*/CIRS measurements at 0.27 mbar. Near 1 mbar, our retrieval results and the other profiles shown in Fig. 14 diverge, which may be indicative of another loss mechanism for CH_3CN in Titan's lower stratosphere that has not been accounted for by photochemical models. At higher pressures (particularly >10 mbar, or <100 km) our retrievals adhere more strongly to the input vertical profiles (Fig. 9), inhibiting us from accurately determining the nature of CH_3CN's lower atmosphere gradient.

Our retrievals are compared to contemporary *Cassini*/CIRS limb (Vinatier et al., 2015) and nadir (Coustenis et al., 2016) measurements in Fig. 15. We measure lower abundances than those found by Coustenis et al. (2016) from 50°N and S nadir observations at the peak of their contribution functions at 7 (HCN) or 10 (HC_3N and C_3H_4) mbar; however, these nadir measurements are assuming constant vertical profiles above condensation altitudes, where our continuous retrievals often manifest as steep gradients in the lower atmosphere. Our results agree better at altitudes above those sounded by 2012 and 2013 CIRS nadir observations, particularly at the altitudes of the secondary peaks in the contribution functions of HCN and HC_3N near 0.1–0.5 mbar seen in 2014.

We find our 2012 HCN profiles (derived from $HC^{15}N$) to be comparable to the CIRS limb measurements by Vinatier et al. (2015) in all regions, with the exception of the south at pressures <0.01 mbar; here, the large latitudinal average of our ALMA beam-footprint measurements may be less directly comparable to CIRS, which is more sensitive to variations in the upper atmosphere. Due to the *Cassini* orbiter's high latitude resolution and preferable viewing geometry, abundance enhancements as a result of subsidence onto the south pole, or the increased formation/decreased destruction of these molecules in southern winter, are more readily apparent. Further, sub-mm observations lose sensitivity in the upper atmosphere (>800 km) for all molecules observed here (Fig. 6). For example, while the northern CIRS profile falls within our retrieval errors, we do not observe the same vertical structure in the upper atmosphere showing a depletion of HCN at pressures <0.02 mbar, as our retrieved profile tends to adhere more strongly to the *a priori* values in the upper atmosphere.

Similar discrepancies are observed for HC_3N, where we find a more shallow gradient at low northern (Center) and southern (South) latitudes at high altitudes compared to the 2012 CIRS retrievals. We might expect that the relatively large ALMA beams may more easily obfuscate spatial variations in shorter lived trace species, such as HC_3N and C_3H_4, which are more susceptible to short term change in atmospheric circulation or increased production as the moon transitions into southern winter. As HC_3N seems to be a good tracer of atmosphere dynamics in Titan's stratosphere (Fig. 1), continued ALMA monitoring of this molecule, particularly with higher spatial resolution, may help elucidate changes in shorter lived nitriles and circulation in the stratosphere.

Due to the lack of earlier spatially resolved C_3H_4 observations, we compare our 2014 retrievals to those of Vinatier et al. (2015) from 2012. Unlike in HCN and HC_3N, the ALMA- and CIRS-derived southern profiles here are in good agreement, as are the measurements from low northern latitudes (Center). The lower altitude enhancement at mid-northern latitudes (North) rises by ∼30 km (from 170–200 km), and increases in magnitude by a factor of 2.8. This may not be unreasonable, as Vinatier et al. (2015) and Coustenis et al. (2016) both observe a general increase in C_3H_4 abundance at mid-northern latitudes into northern spring, and the now reversed pole-to-pole circulation cell may shift a lower atmosphere reservoir of C_3H_4 to higher altitudes. As with the other gases, the abundance measurements derived from ALMA observations comprise multiple latitude decades, making direct comparisons to CIRS limb observations difficult; however, we find that our results are generally compatible with those from *Cassini*, previous ground-based observations, and photochemical model results, particularly near 1–10 mbar, where our retrievals are most sensitive.

4.2 Spatial and Temporal Variations

While abundance comparisons to *Cassini* are generally in agreement, the HCN and HC_3N results show that our ALMA-derived retrievals are missing the variability in vertical gradients and oscillations seen at high latitudes on Titan due to the spatial averaging of the relatively large ALMA beams, the inherent vertical resolution constraints of ground-based (nadir) observations, and the decreased sensitivity to altitudes >300 km. However, our results still display large spatial variations in northern and southern latitudes compared to the low northern (Center) latitudes in both retrieved vertical profiles (Fig. 11–13) and intensity maps (Fig. 1). When plotting profiles from each spatial region over time (Fig. 16), we can also see temporal trends arise as a result of Titan's atmospheric dynamics, even at altitudes where ALMA is less sensitive.

The HCN isotopes that we model here lie on the broadened wings of CO emission lines, making integrated flux maps difficult to interpret. In the retrieval results, we observe a significant enhancement in the north during 2015 near 0.1 mbar, which is ∼16 times greater than the abundance at lower northern latitudes (Center) and a factor of 7 greater than the south. A similar increase of HCN in mid-northern latitudes at similar altitudes was observed in *Cassini*/CIRS limb data between 2011–2012 as the result of the of the weakening northern polar vortex and the advection of accumulated enriched gas to lower latitudes (Vinatier et al., 2015); the upper atmosphere (<0.01 mbar) in these observations was also observed to be depleted in HCN, further reinforcing the notion of a recent upwelling from the recent north-to-south circulation cell. This trend is also present in our observations in 2014 and 2015, indicating we may be probing portions of the upper atmosphere at higher northern latitudes that are now depleted in HCN due to the rise of lower stratospheric air in the ascending branch. Further, the retrieval results show a consistent enhancement of HCN in the upper atmosphere (>300 km) of the low-southern latitudes over time (Fig. 16, top row), resulting in abundances >6 times those of the Center and a factor of 5 greater than the North. While our abundance retrievals are less sensitive to emission at these altitudes, the trend in these profiles seems significant; this trend is also observable at low northern latitudes (Center) at the highest portion of our retrievals (>400 km). Both of these increases are indicative of the circulation of the large concentration of HCN formed at the north pole during northern winter to the south (now winter) pole, and lower latitudes. The effects of this new circulation are present in contemporary *Cassini*/CIRS measurements at high southern latitudes (Vinatier et al., 2015; Coustenis et al., 2016; Sylvestre et al., 2018), where subsidence onto the southern pole greatly increased the abundance of all species. In particular, species with long chemical lifetimes compared to dynamical timescales in Titan's stratosphere (such as HCN; see e.g. Loison et al., 2015) provide good tracers of Titan's global circulation (Vinatier et al., 2015).

Retrievals of HC_3N for each year show significant enhancements in the lower atmosphere in both the North and South profiles, and are the largest spatial enhancements that we measure here. While the North and South enhancements are reduced in 2014 – with 34 and 13 times the Center abundance, respectively – they increase from a factor of 50 and 34 to 75 and 61 compared to the center from 2013 to 2015; these factors are larger than enhancements exhibited by the other nitriles and C_3H_4 by an order of magnitude in the lower stratosphere, but comparable to the large enrichment seen during the northern winter by *Cassini* (Teanby et al., 2010b). These peaks most likely influence the large enhancement seen in the disk-averaged profile from each year (Fig. 10). A northern stratospheric enhancement of HC_3N may be the result of advection between the polar vortex and lower latitudes, but a 'tongue' of enriched gas was not observed for HC_3N during northern winter, as was seen for HCN (Teanby et al., 2008). A rapidly appearing tongue in the south soon after the circulation reversal in 2011 also seems unlikely (but motivates an analysis of the wind speeds during this epoch). Further, lower atmosphere enhancements in abundance are observed by photochemical models due to the influence of galactic cosmic ray (GCR) induced chemistry; yet, the Center retrievals lack an enhanced peak in the lower stratosphere, which would most likely manifest regardless of latitude. This trend also does not fully agree with the integrated intensity maps (Fig. 1), where the enhancements are only a factor of 2–3 compared to the central flux, with a prominent decrease in the north from 2014 to 2015. The shift between a northern and southern enhancement of HC_3N between 2014 and 2015 is consistent across ALMA observations of Titan (Cordiner et al., 2017). The discrepancy between retrieval results and image maps may arise from the high opacity of the HC_3N line core in the sub-mm, possibly inhibiting us from obtaining meaningful comparisons in the lower atmosphere from integrated emission maps (Cordiner et al., 2018). Finally, these spatial enhancements occur at different altitudes – near 150 km in the south and 200 km in the north – and the peak of both regions decreases by about 20 km from 2013 to 2015. The shift of these peaks with altitude and time may be a result of a decrease in stratospheric temperatures, causing the condensation altitude of HC_3N to change; this was observed in *Cassini*/CIRS spectra at the south pole (Jennings et al., 2012; Coustenis et al., 2016). While ALMA temperature measurements at these same spatial regions between 100–200 km reveal cooler temperatures at northern latitudes compared to those from the subsolar point, the temperatures at low southern latitudes are comparable to those of the center (see Paper I, Fig. 9).

HC_3N emission maps show significant spatial changes from 2013 to 2015, where we observe quickly increasing southern flux and decreasing flux in the north, but these large changes aren't immediately obvious in the retrieval results. We do observe a general increase in southern abundances over time above and below the abundance peak at $\sim$ 150 km, and a similar decrease in the north (Fig. 16, second row); we also observe a reduction in abundance from Center retrievals >1 mbar from 2014 to 2015. Thus, we can trace most of the variability in the integrated flux maps to changes in the deeper atmosphere, and altitudes above the potentially enriched reservoir of HC_3N near 1 mbar. The retrieved profiles consistently show higher abundance in the upper atmosphere at low southern latitudes by a factor of 2–4 compared to the North, but the profiles do not show any significant trends over time.

Our HC_3N North and South retrievals (and thus, the disk-averaged results) may be adversely effected by high opacity and large latitudinal averages at low altitudes. As found by Cordiner et al. (2018), these effects may result in abundance underestimates at the pole for higher spatial resolution observations, but HC_3N still provides a valuable tracer of meridional mixing of nitrile reservoirs from Titan's poles. If the enhancements we present here are real, the cause of a lower stratospheric reservoir of HC_3N at mid to low latitudes is not fully understood; this motivates a more in depth study of HC_3N emission over time across Titan's limb, where more accurate abundances may be derived at latitudes below the poles.

As with the nitriles, we observe an enhancement of C_3H_4 at mid-northern latitudes with factors of 5–6 greater than the Center retrievals in 2014 and 2015. Similar to HCN and HC_3N, we find that the Center C_3H_4 abundance decreases with time at altitudes <300 km – particularly from 2014 to 2015 (Fig. 16, third row). We also observe a simultaneous increase in the southern abundances of C_3H_4 by a factor of 2 compared to the Center profiles, and a general increase in the upper atmosphere of both North and South retrievals. Both of these trends are indicative of the redistribution of enriched gas from high northern latitudes to the south with the reversal of Titan's circulation cell, though we do not observe the increase in upper atmosphere gradient observed with CIRS (Vinatier et al., 2015); this latter effect may be missing from our C_3H_4 results due to the lack of sensitivity above ∼400 km (Fig. 6D). While both HC_3N and C_3H_4 did not show a significant lower atmosphere tongue of enriched gas leaking from the polar vortex in *Cassini*/CIRS observations, C_3H_4 did extend further past the vortex boundary than HC_3N by $10-15°$ (Teanby et al., 2009). We also find that C_3H_4 is more enhanced at the Center compared to HC_3N, as measured during northern winter.

CH_3CN shows enhancements in the north in both retrievals (Fig. 16, bottom row) and maps (Fig. 1). In the latter, we see the emission peaks confined to 45–60°N and higher, consistent with some gas advection beyond the northern polar vortex barrier observed with *Cassini* (Teanby et al., 2008). We find a slight increase in lower atmosphere abundances in the North over time, increasing by a factor of 3–6.5 compared to the Center near 1 mbar; this enhancement rises about 30 km from 2013 to 2015. The decrease in northern emission seen in the integrated flux maps may be an artifact caused by the increasing spatial resolution over time, but we do observe a decrease in northern abundance retrievals near 0.01 mbar (400 km) by a factor of ∼3 from 2013 to 2015, where the contribution function for CH_3CN has a secondary peak (Fig. 6E). This change is minor compared to the retrieval errors (i.e. $<2\sigma$), but could be the result of upwelling of depleted air from the lower atmosphere that we see with HCN and as observed by CIRS (Vinatier et al., 2015). The enhancement of CH_3CN in the northern lower atmosphere is indicative of a winter enrichment of this molecule, which may be advected to the lower latitudes after northern winter. CH_3CN has a relatively long chemical lifetime throughout Titan's atmosphere (as compared to the dynamical lifetime), with a similar lifetime to HCN in the stratosphere (Wilson and Atreya, 2004; Loison et al., 2015). However, we don't find large variations in southern abundances at higher altitudes over time, or a large difference between North and South abundances in the upper stratosphere as is observed for HCN here. As with the other nitriles, observations of these changes at the southern pole are inhibited by our viewing angle from Earth, though the emission maps may provide evidence for circulation from the north pole to the south over time.

Vertical oscillations appear in CH_3CN retrievals to a larger extent than the other molecules, particularly in 2014. Oscillations in previous *Cassini* measurements of nitriles have been documented, particularly for mid to high northern latitudes, and are thought to be the result of small scale dynamical mixing between gas-depleted lower latitudes and the enriched polar vortex (Teanby et al., 2009). While our CH_3CN retrievals exhibit larger vertical oscillations with increasing northern latitudes (Fig. 16), we do not see a similar pattern in the other nitriles or C_3H_4, as were seen in *Cassini*/CIRS results (Teanby et al., 2009; Vinatier et al., 2015). The lack of contemporary, spatially resolved abundance measurements for CH_3CN in Titan's stratosphere, combined with the averaging of our measurements across multiple latitudes (with potentially significant dynamics and meridional mixing) makes these vertical oscillations difficult to interpret.

5 Conclusions

Building on the previous results in Paper I, we present vertical abundance profiles of HCN, HC_3N, C_3H_4, and CH_3CN obtained through the analysis of rotational transitions in spatially resolved (beam sizes $\sim 0.2 - 0.5''$) ALMA flux calibration data from 2012 to 2015. The comparison of three regions on Titan's disk (centered at ∼48°N, 21°N, and 16°S) reveal distinct spatial variations and insight into Titan's atmospheric dynamics. In contrast with the temperature profiles presented in Paper I, the abundance profiles of these molecules show temporal changes over the 3 years of observation from 2012 to 2015. The combination of the spatial and temporal variations we observe informs our understanding of Titan's atmospheric circulation into northern spring and summer. Our findings are summarized as follows:

- All four molecules display enhancements in the North (and often the South) compared to Center, ranging from factors of ∼6 in C_3H_4 and CH_3CN to 15 and 75 in HCN and HC_3N, respectively. Southern enhancements are more noticeable in the upper atmosphere, particularly for HCN and HC_3N, yet do not exhibit the steep vertical gradients seen by *Cassini*/CIRS (Teanby et al., 2012; Vinatier et al., 2015; Coustenis et al., 2016).

- We find large enhancements of HC_3N between 150–200 km in all North and South retrievals. This is indicative of a relatively new lower atmosphere HC_3N reservoir, but may also be the result of opacity effects of sub-mm HC_3N lines (Cordiner et al., 2018). Nevertheless, the combination of retrieval results and integrated flux maps show a rapid reduction of HC_3N at Titan's north pole and a simultaneous increase in the south between 2013 and 2015.

- We observe many temporal trends in abundance retrievals that reveal the continued effects of Titan's large north-to-south circulation cell:

  i. The increase of southern HCN, HC_3N, C_3H_4, and potentially CH_3CN at higher altitudes, and similar trends (with reduced magnitude) at low-northern latitudes (Center).

  ii. A slight increase in the abundances of mid northern latitudes over time in HCN, C_3H_4, CH_3CN, with a change in upper atmosphere gradients in the longer lived chemical species (HCN and CH_3CN).

  iii. An increase in abundance for all molecules at pressures >1 mbar at southern latitudes, except CH_3CN, which does not effectively sound higher pressures.

  iv. A reduction in abundance for all molecules in Center profiles at pressures >0.1 mbar.

  These trends show evidence for subsidence at the southern pole, the decrease of a 'tongue' at low northern latitudes (where enriched air was advected from the northern polar vortex during winter), and lofted air replete with longer lived chemical species from Titan's lower stratosphere to higher altitudes.

– The polar enhancements and vertical gradients observed are generally less significant than those observed with the *Cassini* orbiter, indicating that the effects of atmospheric chemistry and dynamics are muted when observed in large latitudinal averages (as seen with the temperatures reported in Paper I).

We validated our results using contemporaneous *Cassini*/CIRS data, and through comparisons of mean profiles from 2012 to 2015 to previous disk-averaged ground-based observations and photochemical model results. We find that our retrieved profiles are comparable to contemporary studies with the exception of HC_3N, which is optically thick at the poles where the molecule has been observed to be greatly enhanced. However, the large temporal variations and fine vertical structure observed with the *Cassini* orbiter are obscured by the latitudinal averaged measurements derived from spectra representing relatively large ALMA beam-footprints, particularly at higher altitudes where sub-mm measurements are not as sensitive, as observed with the previous atmospheric temperature retrievals (Paper I). Thus, this work serves as a proof of concept for future measurements of Titan's chemical abundances throughout the stratosphere that will allow us to continue monitoring Titan's varied atmospheric dynamics into the post-*Cassini* era.

6 Acknowledgments

This research was supported by NASA's Office of Education and the NASA Minority University Research and Education Project ASTAR/JGFP Grant #NNX15AU59H. Additional funding was provided by the NRAO Student Observing Support award #SOSPA3-012. C.A.N was supported in this work by the NASA Solar System Observations Program and the NASA Astrobiology Institute. M.A.C received funding from the National Science Foundation under Grant No. AST-1616306. N.A.T and P.G.J.I were supported by the UK Science and Technology Facilities Council. S.B.C was funded by an award from the NASA Science Innovation Fund. This paper makes use of the following ALMA data: ADS/JAO.ALMA#2011.0.00724.S, 2011.0.00820.S, 2012.1.00377.S, 2012.1.00225.S, 2012.1.00453.S, 2013.1.00220.S, and 2013.1.00111.S. ALMA is a partnership of ESO (representing its member states), NSF (USA) and NINS (Japan), together with NRC (Canada) and NSC and ASIAA (Taiwan) and KASI (Republic of Korea), in cooperation with the Republic of Chile. The Joint ALMA Observatory is operated by ESO, AUI/NRAO and NAOJ. The National Radio Astronomy Observatory is a facility of the National Science Foundation operated under cooperative agreement by Associated Universities, Inc.

The authors would like to thank Richard Achterberg for his insightful comments on Titan's stratospheric temperatures and his contribution of *Cassini*/CIRS temperature profiles for this work and Paper I.

References

Achterberg, R. K., Gierasch, P. J., Conrath, B. J., Flasar, F. M., and Nixon, C. A. (2011). "Temporal variations of Titan's middle-atmosphere temperatures from 2004 to 2009 observed by Cassini/CIRS". In: *Icarus* 211, pp. 686–698.

Achterberg, R. K., Gierasch, P. J., Conrath, B. J., Flasar, F. M., Jennings, D. E., and Nixon, C. A. (2014). "Post-equinox variations of Titan's mid-stratospheric temperatures from Cassini/CIRS observations". In: *DPS Meeting #46*.

Bézard, B., Marten, A., and Paubert, G. (1992). "First Ground-based Detection of Cyanoacetylene on Titan". In: *AAS/Division for Planetary Sciences Meeting Abstracts #24*. Vol. 24. Bulletin of the American Astronomical Society, p. 953.

— (1993). "Detection of Acetonitrile on Titan". In: *AAS/Division for Planetary Sciences Meeting Abstracts #25*. Vol. 25. Bulletin of the American Astronomical Society, p. 1100.

Bézard, B., Yelle, R., and Nixon, C. A. (2014). "The Composition of Titan's atmosphere". In: *Titan*. Ed. by I. Müller-Wodarg, C. A. Griffith, E. Lellouch, and T. E. Cravens. Cambridge, UK: Cambridge University Press, p. 158.

Broadfoot, A. L. et al. (1981). "Extreme ultraviolet observations from Voyager 1 encounter with Saturn". In: *Science* 212, pp. 206–211. DOI: 10.1126/science.212.4491.206.

Cordiner, M. A. et al. (2014). "ALMA measurements of the HNC and HC_3N distributions in Titan's atmosphere". In: *ApJ* 795, pp. L30–L35.

Cordiner, M. A. et al. (2015). "Ethyl cyanide on Titan: spectroscopic detection and mapping using ALMA". In: *ApJ* 800, pp. L14–L19.

Cordiner, M. A. et al. (2017). "ALMA observations of Titan's atmospheric chemistry and seasonal variation". In: *IAU Symposium: Astrochemistry VII - Through the Cosmos from Galaxies to Planets*. Vol. 332. Cambridge University Press (In Press).

Cordiner, M. A., Nixon, C. A., Charnley, S. B., Teanby, N. A., Kisiel, Z., and Vuitton, V. (2018). "Interferometric imaging of Titan's HC_3N, $H^{13}CCCN$ and $HCCC^{15}N$". In: *ApJ* 859, p. L15. DOI: 10.3847/2041-8213/aac38d.

Coustenis, A. and Bezard, B. (1995). "Titan's atmosphere from Voyager infrared observations. 4: Latitudinal variations of temperature and composition". In: *Icarus* 115, pp. 126–140. DOI: 10.1006/icar.1995.1084.

Coustenis, A. et al. (2016). "Titan's temporal evolution in stratospheric trace gases near the poles". In: *Icarus* 270, pp. 409–420.

Dobrijevic, M. and Loison, J. C. (2018). "The photochemical fractionation of nitrogen isotopologues in Titan's atmosphere". In: *Icarus* 307, pp. 371–379. DOI: 10.1016/j.icarus.2017.10.027.

Dudaryonok, A. S., Lavrentieva, N. N., and Buldyreva, J. V. (2015). "N_2-broadening coefficients of CH_3CN rovibrational lines and their temperature dependence for the Earth and Titan atmospheres". In: *Icarus* 256, pp. 30–36. DOI: 10.1016/j.icarus.2015.04.025.

Flasar, F. M., Samuelson, R. E., and Conrath, B. J. (1981). "Titan's atmosphere: temperature and dynamics". In: *Nature* 292, pp. 293–298.

Flasar, F. M. et al. (2005). "Titan's atmospheric temperatures, winds, and composition". In: *Science* 308, pp. 975–978.

Gillett, F. C. (1975). "Further observations of the 8-13 micron spectrum of Titan". In: *ApJL* 201, pp. L41–L43. DOI: 10.1086/181937.

Gillett, F. C., Forrest, W. J., and Merrill, K. M. (1973). "8-13 Micron Observations of Titan". In: *ApJL* 184, p. L93. DOI: 10.1086/181296.

Gordon, I. E. et al. (2017). "The HITRAN2016 molecular spectroscopic database". In: *J. Quant. Spec. Radiat. Transf.* 203, pp. 3–69. DOI: 10.1016/j.jqsrt.2017.06.038.

Gurwell, M. (2004). "Submillimeter observations of Titan: global measures of stratospheric temperature, CO, HCN, HC_3N, and the isotopic ratios of $^{12}C/^{13}C$ and $^{14}N/^{15}N$". In: *ApJ* 616, pp. L7–L10.

Hanel, R. et al. (1981). "Infrared observations of the Saturnian system from Voyager 1". In: *Science* 212, pp. 192–200. DOI: 10.1126/science.212.4491.192.

Hörst, S. M. (2017). "Titan's atmosphere and climate". In: *Journal of Geophysical Research (Planets)* 122, pp. 432–482. DOI: 10.1002/2016JE005240.

Irwin, P. G. J. et al. (2008). “The NEMESIS planetary atmosphere radiative transfer and retrieval tool”. In: *J. Quant. Spec. Radiat. Transf.* 109, pp. 1136–1150.

Jennings, D. E. et al. (2012). “Seasonal Disappearance of Far-infrared Haze in Titan’s Stratosphere”. In: *ApJ* 754, p. L3. DOI: 10.1088/2041-8205/754/1/L3.

Krasnopolsky, V. A. (2014). “Chemical composition of Titan’s atmosphere and ionosphere: observations and the photochemical model”. In: *Icarus* 236, pp. 83–91.

Kuiper, G. P. (1944). “Titan: a Satellite with an Atmosphere.” In: *ApJ* 100, p. 378. DOI: 10.1086/144679.

Kunde, V. G., Aikin, A. C., Hanel, R. A., Jennings, D. E., Maguire, W. C., and Samuelson, R. E. (1981). “C4H2, HC3N and C2N2 in Titan’s atmosphere”. In: *Nature* 292, pp. 686–688. DOI: 10.1038/292686a0.

Lai, J. C.-Y. et al. (2017). “Mapping Vinyl Cyanide and Other Nitriles in Titan’s Atmosphere Using ALMA”. In: *AJ* 154, p. 206. DOI: 10.3847/1538-3881/aa8eef.

Lavvas, P., Griffith, C. A., and Yelle, R. V. (2011). “Condensation in Titan’s atmosphere at the Huygens landing site”. In: *Icarus* 215, pp. 732–750. DOI: 10.1016/j.icarus.2011.06.040.

Lellouch, E., Romani, P. N., and Rosenqvist, J. (1994). “The vertical Distribution and Origin of HCN in Neptune’s Atmosphere”. In: *Icarus* 108, pp. 112–136. DOI: 10.1006/icar.1994.1045.

Loison, J. C. et al. (2015). “The neutral photochemistry of nitriles, amines and imines in the atmosphere of Titan”. In: *Icarus* 247, pp. 218–247.

Maguire, W. C., Hanel, R. A., Jennings, D. E., Kunde, V. G., and Samuelson, R. E. (1981). “C3H8 and C3H4 in Titan’s atmosphere”. In: *Nature* 292, pp. 683–686. DOI: 10.1038/292683a0.

Marten, A., Hidayat, T., Biraud, Y., and Moreno, R. (2002). “New millimeter heterodyne observations of Titan: vertical distributions of nitriles HCN, HC_3N, CH_3CN, and the isotopic ratio $^15N/^14N$ in its atmosphere”. In: *Icarus* 158, pp. 532–544.

Molter, E. M. et al. (2016). “ALMA observations of HCN and its isotopologues on Titan”. In: *AJ* 152 (42), pp. 1–7.

Müller, H. S. P., Schlöder, F., Stutzki, J., and Winnewisser, G. (2005). “The Cologne Database for Molecular Spectroscopy, CDMS: a useful tool for astronomers and spectroscopists”. In: *Journal of Molecular Structure* 742, pp. 215–227. DOI: 10.1016/j.molstruc.2005.01.027.

Nixon, C. A. et al. (2010). “Upper limits for undetected trace species in the stratosphere of Titan”. In: *Faraday Discuss.* 147, pp. 65–81.

Nixon, C. A. et al. (2013). “Detection of propene in Titan’s stratosphere”. In: *ApJ* 776, pp. L14–L19.

Palmer, Maureen Y. et al. (2017). “ALMA detection and astrobiological potential of vinyl cyanide on Titan”. In: *Sci. Adv.* 3.7. DOI: 10.1126/sciadv.1700022.

Paubert, G., Gautier, D., and Courtin, R. (1984). “The millimeter spectrum of Titan - Detectability of HCN, HC3N, and CH3CN and the CO abundance”. In: *Icarus* 60, pp. 599–612. DOI: 10.1016/0019-1035(84)90167-2.

Paubert, G., Marten, A., Rosolen, C., Gautier, D., and Courtin, R. (1987). “First radiodetection of HCN on Titan.” In: *Bulletin of the American Astronomical Society.* Vol. 19, p. 633.

Raulin, F., Mourey, D., and Toupance, G. (1982). “Organic syntheses from CH_4-N_2 atmospheres: Implications for Titan”. In: *Origins of Life* 12, pp. 267–279. DOI: 10.1007/BF00926897.

Schinder, P. J. et al. (2012). “The structure of Titan’s atmosphere from Cassini radio occultations: occultations from the Prime and Equinox missions”. In: *Icarus* 221, pp. 1020–1031.

Serigano, J., Nixon, C. A., Cordiner, M. A., Irwin, P. G. J., Teanby, N. A., Charnley, S. B., and Lindberg, J. E. (2016). “Isotopic ratios of carbon and oxygen in Titan’s CO using ALMA”. In: *ApJ* 821, pp. L8–L13.

Sylvestre, M., Teanby, N. A., Vinatier, S., Lebonnois, S., and Irwin, P. G. J. (2018). "Seasonal evolution of C_2N_2, C_3H_4, and C_4H_2 abundances in Titan's lower stratosphere". In: *A&A* 609, A64. DOI: 10.1051/0004-6361/201630255.

Teanby, N. A. et al. (2007). "Vertical profiles of HCN, HC_3N, and C_2N_2 in Titan's atmosphere derived from Cassini/CIRS data". In: *Icarus* 186, pp. 364–384.

Teanby, N. A. et al. (2008). "Titan's winter polar vortex structure revealed by chemical tracers". In: *J. Geophys. Res.* 113 (E12003), pp. 1–13.

Teanby, N. A., Irwin, P. G. J., de Kok, R., and Nixon, C. A. (2009). "Dynamical implications of seasonal and spatial variations in Titan's stratospheric composition". In: *Phil. Trans. R. Soc. A* 367, pp. 697–711.

Teanby, N. A., de Kok, R., and Irwin, P. G. J. (2009). "Small-scale composition and haze layering in Titan's polar vortex". In: *Icarus* 204, pp. 645–657. DOI: 10.1016/j.icarus.2009.07.027.

Teanby, N. A., Irwin, P. G. J., de Kok, R., and Nixon, C. A. (2010a). "Seasonal changes in Titan's polar trace gas abundance observed by Cassini". In: *ApJ* 724, pp. L84–L89.

— (2010b). "Mapping Titan's HCN in the far infra-red: implications for photochemistry". In: *Faraday Discuss.* 147, pp. 51–64.

Teanby, N. A. et al. (2012). "Active upper-atmosphere chemistry and dynamics from polar circulation reversal on Titan". In: *Nature* 491, pp. 732–735.

Teanby, N. A. et al. (2013). "Constraints on Titan's middle atmosphere ammonia abundance from Herschel/SPIRE sub-millimetre spectra". In: *Planet. Space Sci.* 75, pp. 136–147.

Teanby, N. A. et al. (2018). "The origin of Titan's external oxygen: further constraints from ALMA upper limits on CS and CH_2NH". In: *AJ* 155, p. 251. DOI: 10.3847/1538-3881/aac172.

Thelen, A. E. et al. (2018). "Spatial variations in Titan's atmospheric temperature: ALMA and Cassini comparisons from 2012 to 2015". In: *Icarus* 307, pp. 380–390. DOI: 10.1016/j.icarus.2017.10.042.

Vinatier, S. et al. (2007). "Vertical abundance profiles of hydrocarbons in Titan's atmosphere at 15 S and 80 N retrieved from Cassini/CIRS spectra". In: *Icarus* 188, pp. 120–138.

Vinatier, S. et al. (2015). "Seasonal variations in Titan's middle atmosphere during the northern spring derived from Cassini/CIRS observations". In: *Icarus* 250, pp. 95–115.

Vuitton, V., Dutuit, O., Smith, M. A., and Balucani, N. (2014). "Chemistry of Titan's atmosphere". In: *Titan*. Ed. by I. Müller-Wodarg, C. A. Griffith, E. Lellouch, and T. E. Cravens. Cambridge, UK: Cambridge University Press, p. 224.

Wilson, E. H. and Atreya, S. K. (2004). "Current state of modeling the photochemistry of Titan's mutually dependent atmosphere and ionosphere". In: *J. Geophys. Res.* 109 (E06002), pp. 1–39.

Yelle, R. V. (1991). "Non-LTE models of Titan's upper atmosphere". In: *ApJ* 383, pp. 380–400. DOI: 10.1086/170796.

Yung, Y. L. (1987). "An update of nitrile photochemistry on Titan". In: *Icarus* 72, pp. 468–472. DOI: 10.1016/0019-1035(87)90186-2.

Table 1: Observational Parameters

Project ID	Observation Date	# of Antennas	Integration Time (s)	Spectral Res. (kHz)	Beam Size[a]	Species
2012						
2011.0.00724.S	05 Jun 2012	21	236	976	0.32″ × 0.25″	$HC^{15}N$
2013						
2011.0.00820.S	01 Jan 2013	24	66	976	0.66″ × 0.53″	C_3H_4
2012.1.00377.S	01 Jun 2013	30	157	976	0.65″ × 0.33″*	HC_3N
					0.50″ × 0.35″*	CH_3CN
2014						
2012.1.00225.S	14 Apr 2014	34	158	976	0.29″ × 0.20″	$H^{13}CN$
2012.1.00453.S	28 Apr 2014	35	158	976	0.37″ × 0.30″*	$HC^{15}N$
	08 Jul 2014	31	157	976	0.45″ × 0.36″	CH_3CN
	16 Jul 2014	32	157	976	0.36″ × 0.35″	HC_3N
					0.38″ × 0.36″	C_3H_4
2015						
2012.1.00377.S	19 May 2015	37	157	976	0.26″ × 0.22″	$H^{13}CN$
					0.25″ × 0.24″	CH_3CN
2013.1.00220.S	14 Jun 2015	41	157	1953	0.38″ × 0.36″*	C_3H_4, C_2H_5CN
2013.1.00111.S	22 Jul 2015	44	261	976	0.35″ × 0.30″*	HC_3N

Notes: [a]FWHM of the Gaussian restoring beam. *Denotes resolution obtained through Briggs weighting as opposed to Natural.

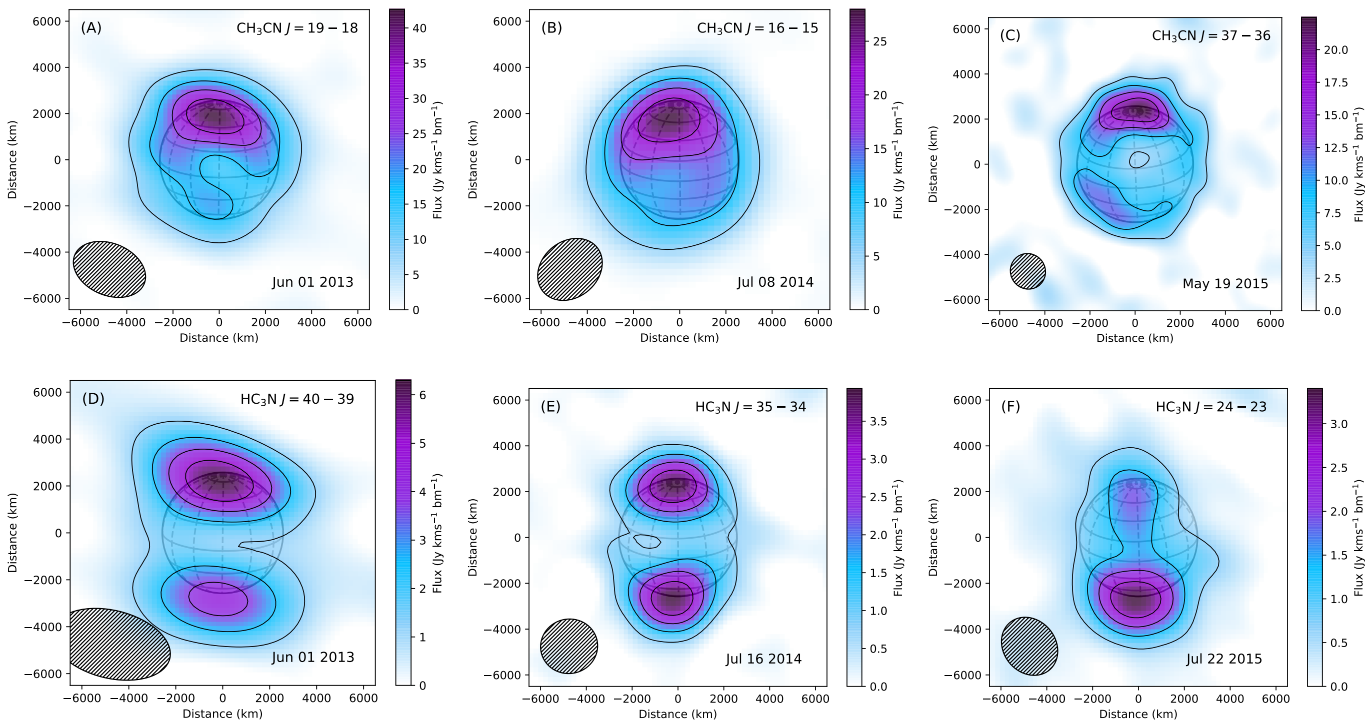

Figure 1: Maps of integrated flux for CH_3CN (A–C) and HC_3N (D–F) lines from 2013, 2014, and 2015. Contours are in intervals of $F_m/5$ (where F_m is the maximum flux of each image cube). The solid gray circle denotes Titan's surface, with lines for latitude (solid) and longitude (dashed) in 22.5° and 30° increments, respectively. Hashed ellipses represent the FWHM of the Gaussian restoring beam for each ALMA observation (see Table 1).

Table 2: Spectral Transitions

Species	**Transition** ($J''_{K''_{a,c}} - J'_{K'_{a,c}}$)	**Rest Freq. (GHz)**
2012		
$HC^{15}N$	8–7	688.273
2013		
C_3H_4	15_3–14_3	256.293
C_3H_4	15_2–14_2	256.317
C_3H_4	15_1–14_1	256.332
C_3H_4	15_0–14_0	256.337
HC_3N	40–39	363.785
CH_3CN	19_6–18_6	349.212
CH_3CN	19_5–18_5	349.286
CH_3CN	19_4–18_4	349.346
CH_3CN	19_3–18_3	349.393
CH_3CN	19_2–18_2	349.426
CH_3CN	19_1–18_1	349.446
CH_3CN	19_0–18_0	349.453
2014		
$H^{13}CN$	8–7	690.552
$HC^{15}N$	4–3	344.200
CH_3CN	16_4–15_4	294.212
CH_3CN	16_3–15_3	294.251
CH_3CN	16_2–15_2	294.280
CH_3CN	16_1–15_1	294.297
CH_3CN	16_0–15_0	294.302
HC_3N	35–34	318.341
C_3H_4	18_4–17_4	307.489
C_3H_4	18_3–17_3	307.530
C_3H_4	18_2–17_2	307.560
C_3H_4	18_1–17_1	307.577
C_3H_4	18_0–17_0	307.583
2015		
$H^{13}CN$	8–7	690.552
CH_3CN	37_3–36_3	679.831
CH_3CN	37_2–36_2	679.895
CH_3CN	37_1–36_1	679.934
CH_3CN	37_0–36_0	679.947
C_3H_4	20_3–19_3	341.682
C_3H_4	20_2–19_2	341.715
C_3H_4	20_1–19_1	341.735
C_3H_4	20_0–19_0	341.741
C_2H_5CN	$40_{1,40}$–$39_{1,39}$	341.704
C_2H_5CN	$40_{0,40}$–$39_{0,39}$	341.711
HC_3N	24–23	218.325

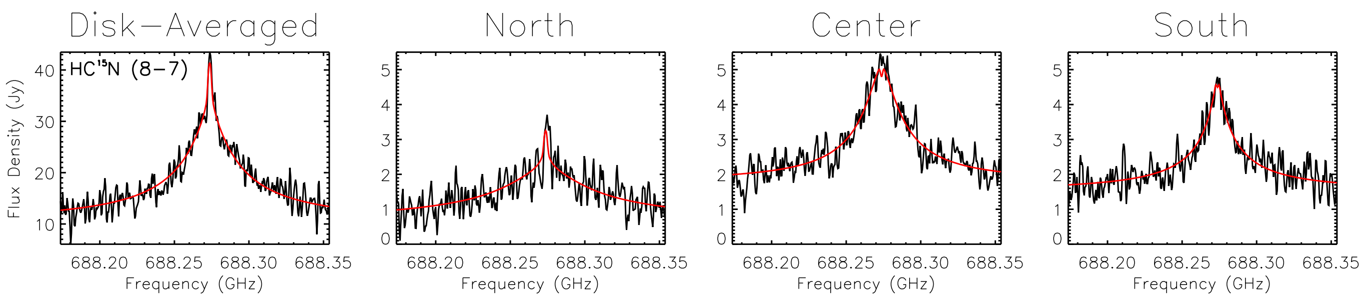

Figure 2: Disk-averaged (first panel), northern (second), central (third), and southern (fourth) ALMA spectra (black) and synthetic best fit spectra (red) are shown for 2012 $HC^{15}N$ emission lines. Spatial spectra are shown on the same y-axis scale to illustrate differences in flux density between various latitudinal regions.

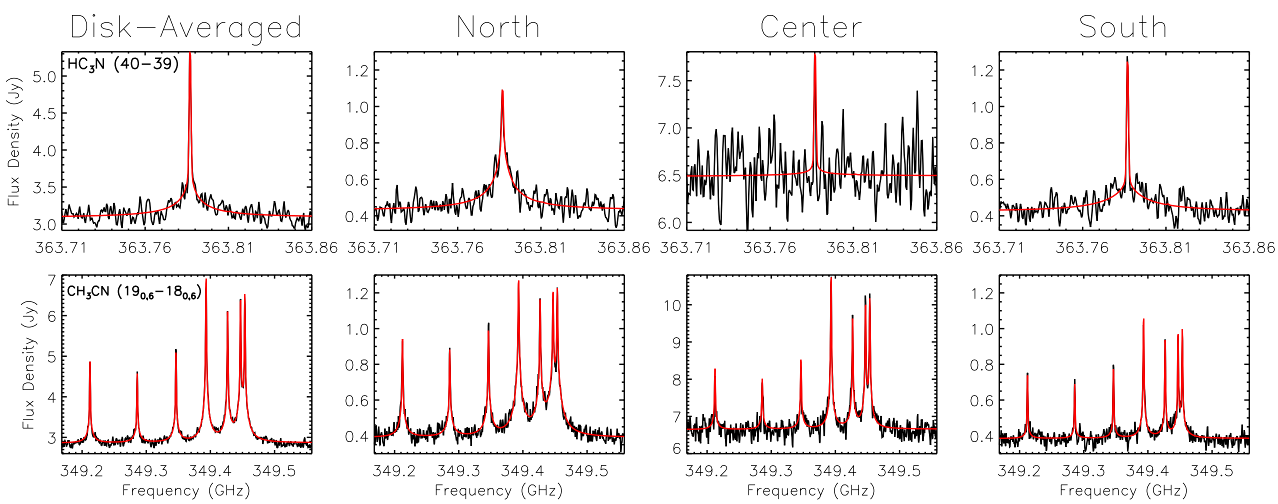

Figure 3: 2013 spectra and best fit models are shown for HC_3N (top row), and CH_3CN (bottom) as in Fig. 2. Center spectra are on a different y-axis scale than the other spatial spectra due to the large variations in flux density as a function of beam size.

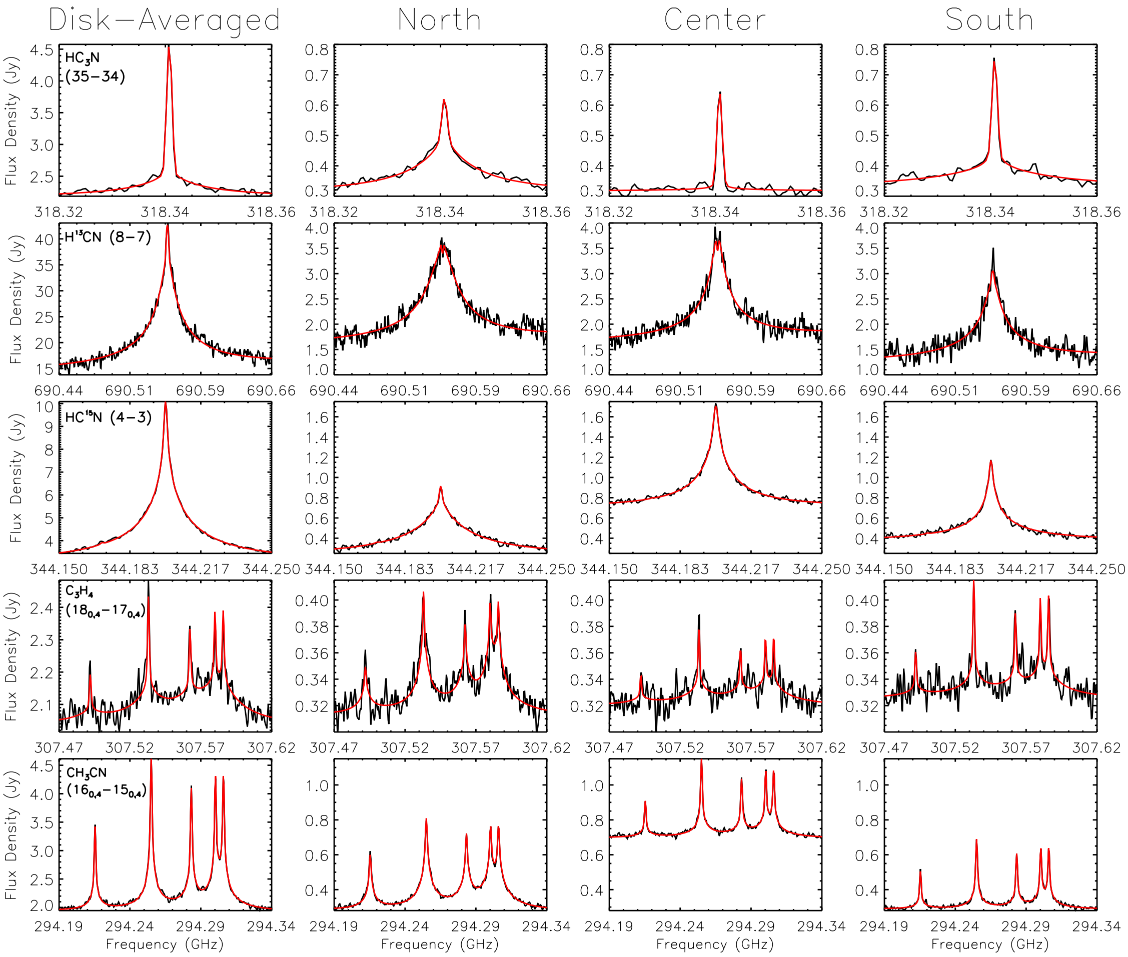

Figure 4: 2014 spectra and best fit models are shown for HC_3N (first row), $H^{13}CN$ (second), $HC^{15}N$ (third), C_3H_4 (fourth), and CH_3CN (fifth) as in Fig. 2.

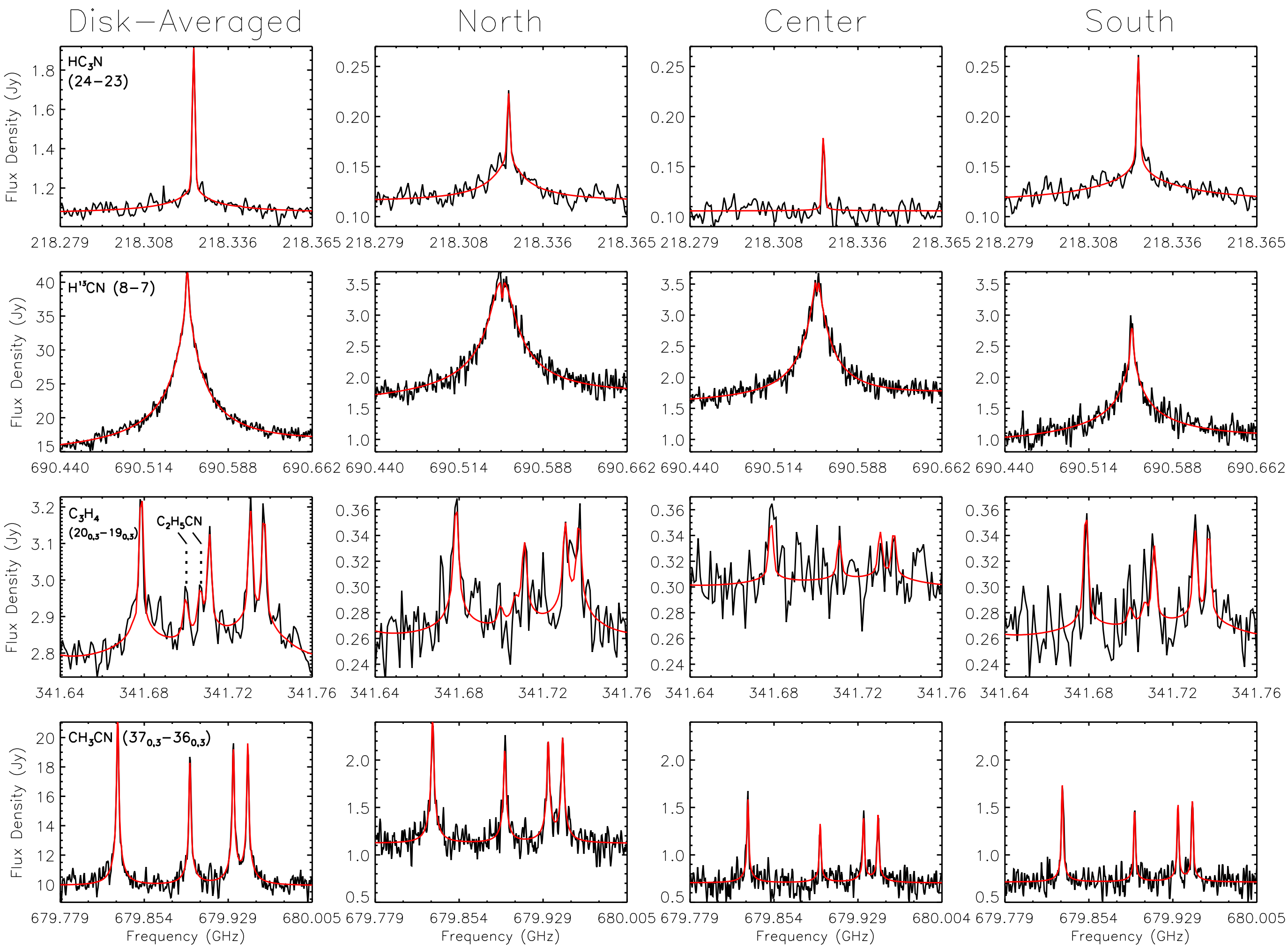

Figure 5: 2015 spectra and best fit models are shown for HC_3N (first row), $H^{13}CN$ (second), C_3H_4 (third), and CH_3CN (fourth) as in Fig. 2. Interloping C_2H_5CN lines in the C_3H_4 spectra are shown with dotted lines in the disk-averaged panel.

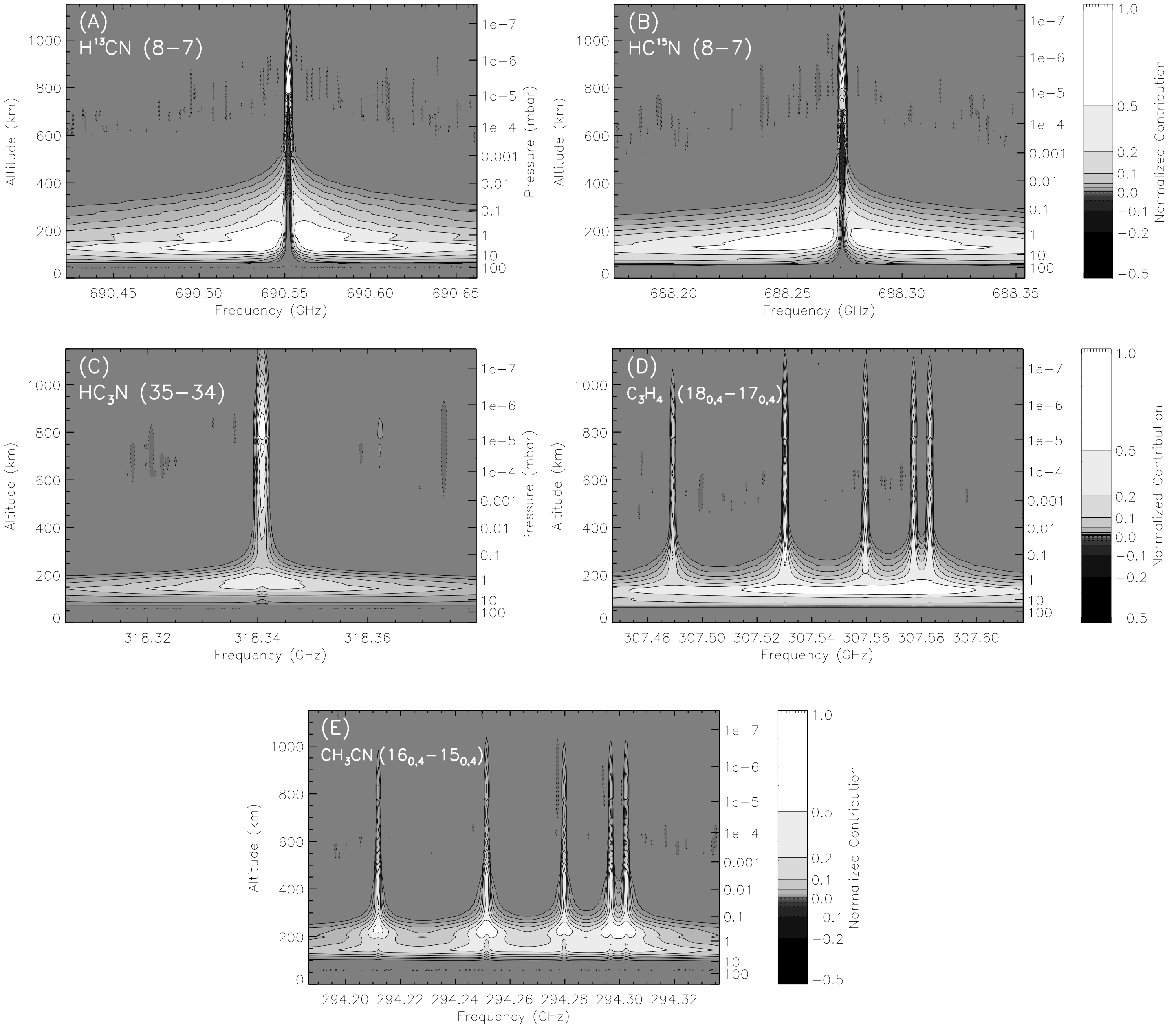

Figure 6: Contours of normalized functional derivatives (Irwin et al., 2008) of spectral radiance per wavenumber with respect to chemical abundance for disk-averaged spectra of $H^{13}CN$ (A), $HC^{15}CN$ (B), HC_3N (C), C_3H_4 (D), and CH_3CN (E), as in Paper I and Molter et al. (2016). Contour levels are 0, ± 0.0046, ± 0.01, ± 0.0215, ± 0.046, ± 0.1, ± 0.215, and ± 0.46, and express molecular line sensitivity to volume mixing ratio at various pressure and altitude values.

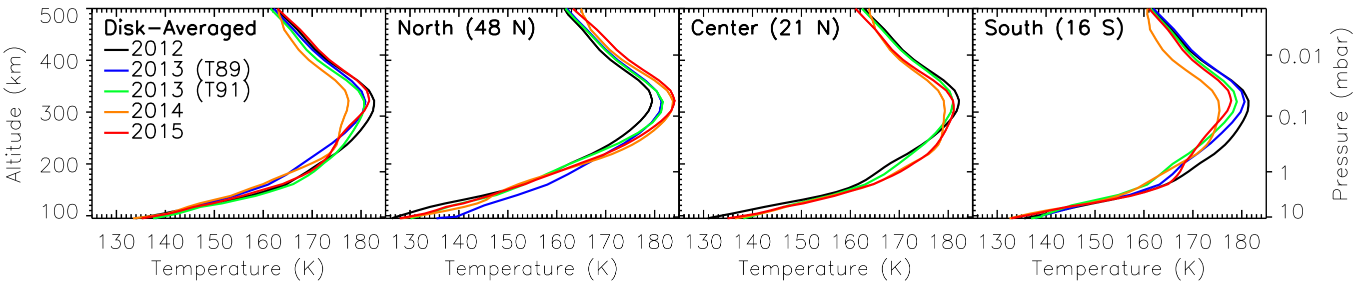

Figure 7: Temperature profiles from Paper I from 2012 (black), 2014 (orange), and 2015 (red), and from the *Cassini* T89 (blue) and T91 (green) flybys from Achterberg et al. (2014).

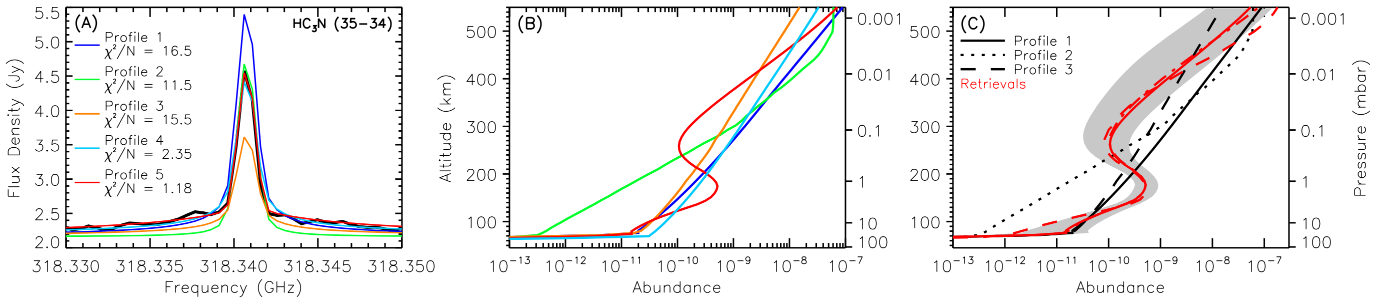

Figure 8: Retrieval tests for HC_3N disk-averaged spectrum from 2014. (A) ALMA spectrum (black) and synthetic spectra for a variety of *a priori* and retrieved profiles: 1, blue) linear gradient; 2, green) profile from Marten et al. (2002); 3, orange) fractional scale height model from Cordiner et al. (2014); 4, teal) fractional scale height retrieval; 5, red) continuous retrieval. (B) Abundance profiles corresponding to spectra in A. (C) Comparison of retrieved profiles (red) using profiles 1-3 as *a priori* guesses (black). The retrieval errors for profile 1 (solid, red) are shown in gray.

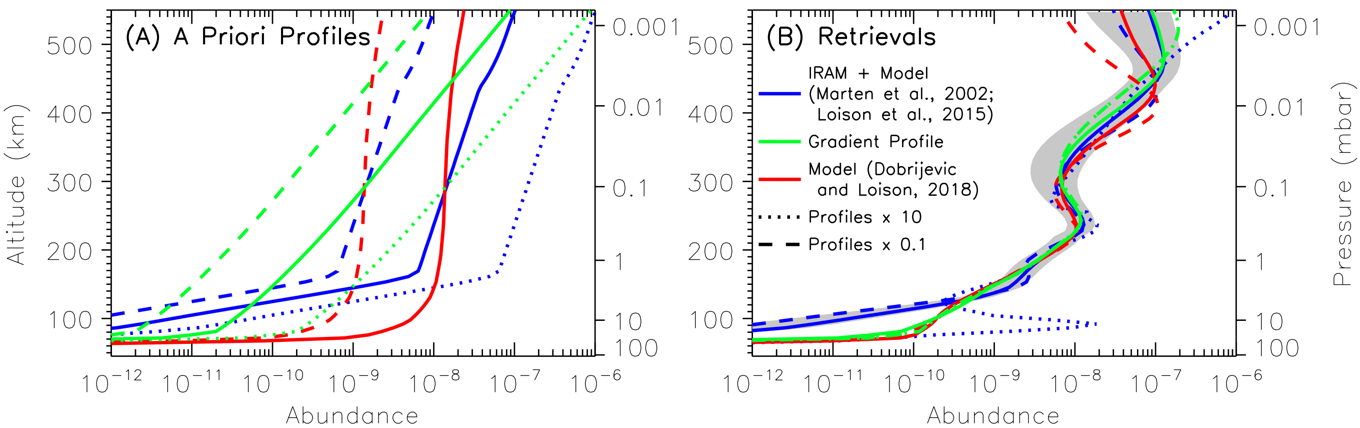

Figure 9: Retrieval tests for the CH_3CN disk-averaged spectrum from 2014. (A) Plot of *a priori* abundance profiles: (blue line) combination of sub-mm observations (Marten et al., 2002) and photochemical model results (Loison et al., 2015); (red line) Dobrijevic and Loison (2018) photochemical model; (green line) a test gradient profile. Dashed lines correspond to 10% of the solid line abundances; dotted lines are profiles with 10× the solid line abundances. (B) Retrieval results for each of the *a priori* profiles in A. The error envelope for the solid blue retrieval (combination of Marten et al., 2002 and Loison et al., 2015) is shown in gray. Retrieved profiles return to *a priori* inputs above and below where the CH_3CN retrievals are sensitive ($\sim 150 - 450$ km, see Fig. 6E).

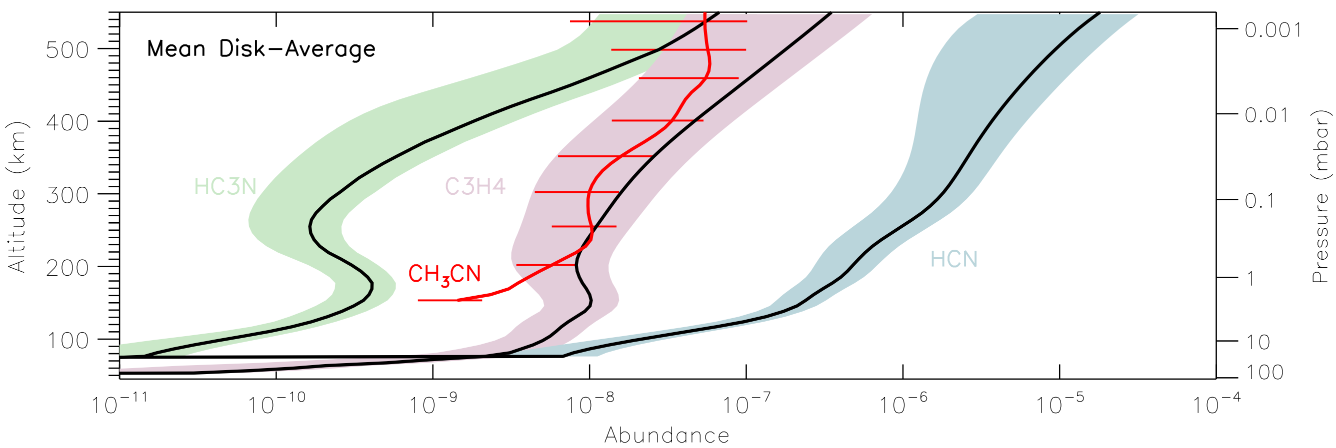

Figure 10: Disk-averaged abundance profiles found by taking the mean of measurements from each year. The HCN profile is an average of both scaled $H^{13}CN$ and $HC^{15}N$ retrievals. Retrieval errors are shown as shaded regions for HCN (blue), HC_3N (green), and C_3H_4 (lilac), and as bars for CH_3CN (red).

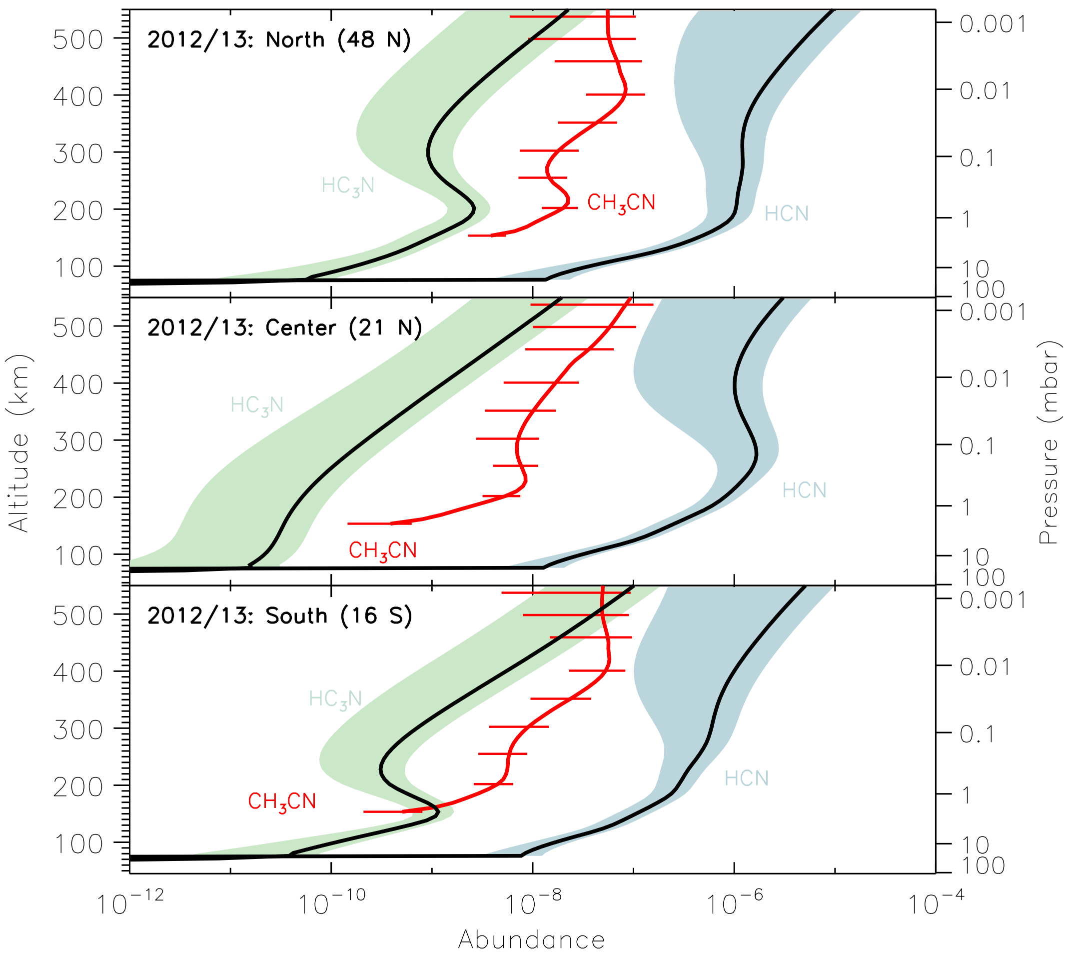

Figure 11: Abundance profiles from retrievals of 2012 and 2013 spectra in Fig. 2 and 3. Retrieval errors are shown as shaded regions, except for bars corresponding to CH_3CN. $HC^{15}N$ abundances have been scaled by the $^{14}N/^{15}N$ ratio = 72.2 from Molter et al. (2016) to represent HCN here.

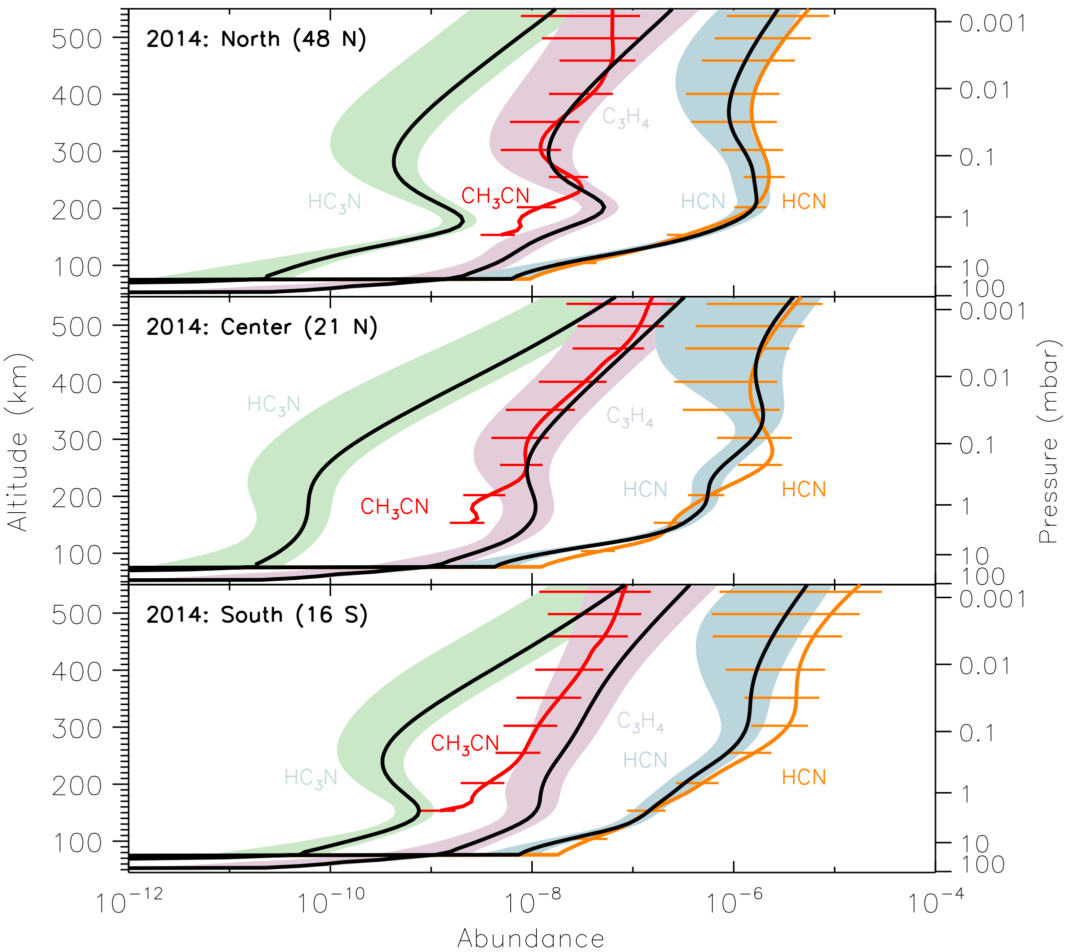

Figure 12: Abundance profiles for 2014 as in Fig. 11. HCN abundances derived from $HC^{15}N$ are shown in black with blue envelopes, and profiles derived from $H^{13}CN$ are shown in orange with error bars, scaled by the $^{12}C/^{13}C$ ratio = 89.8 from Molter et al. (2016).

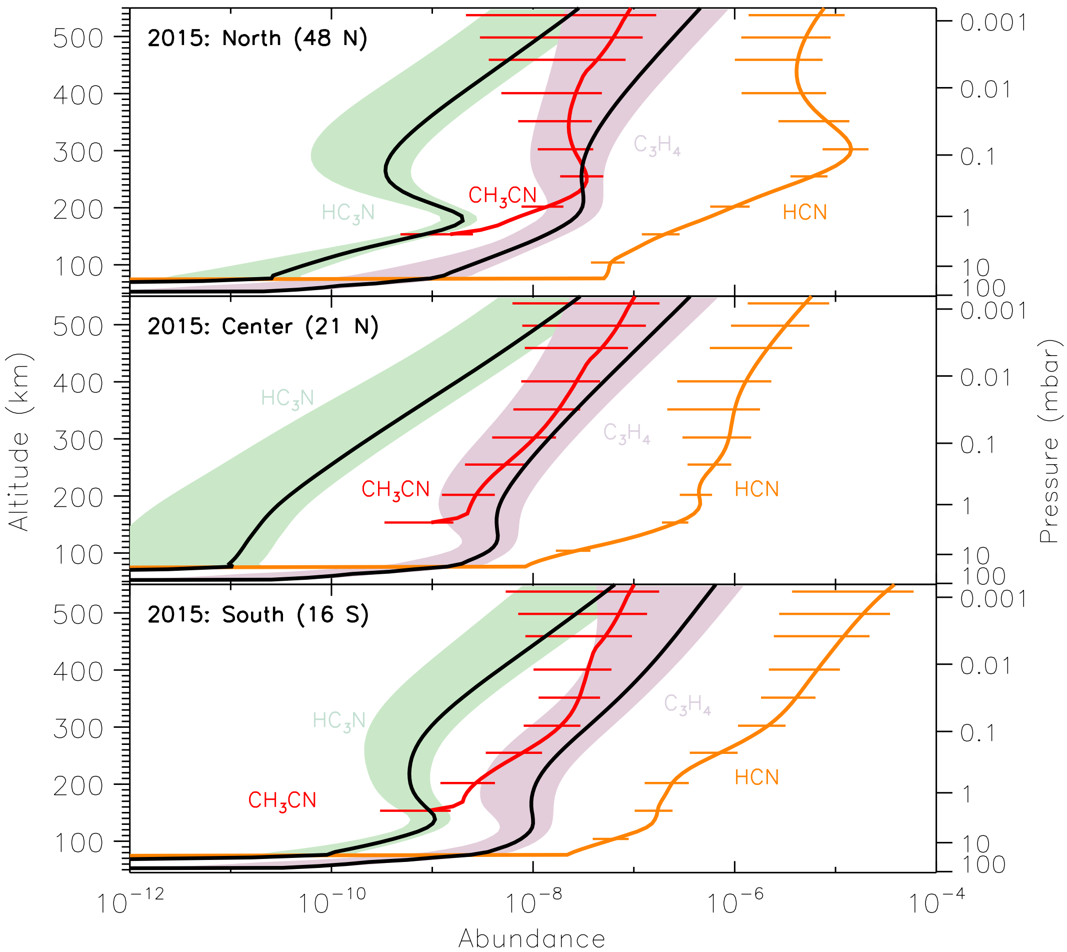

Figure 13: Abundance profiles for 2015, as in Fig. 11 and 12.

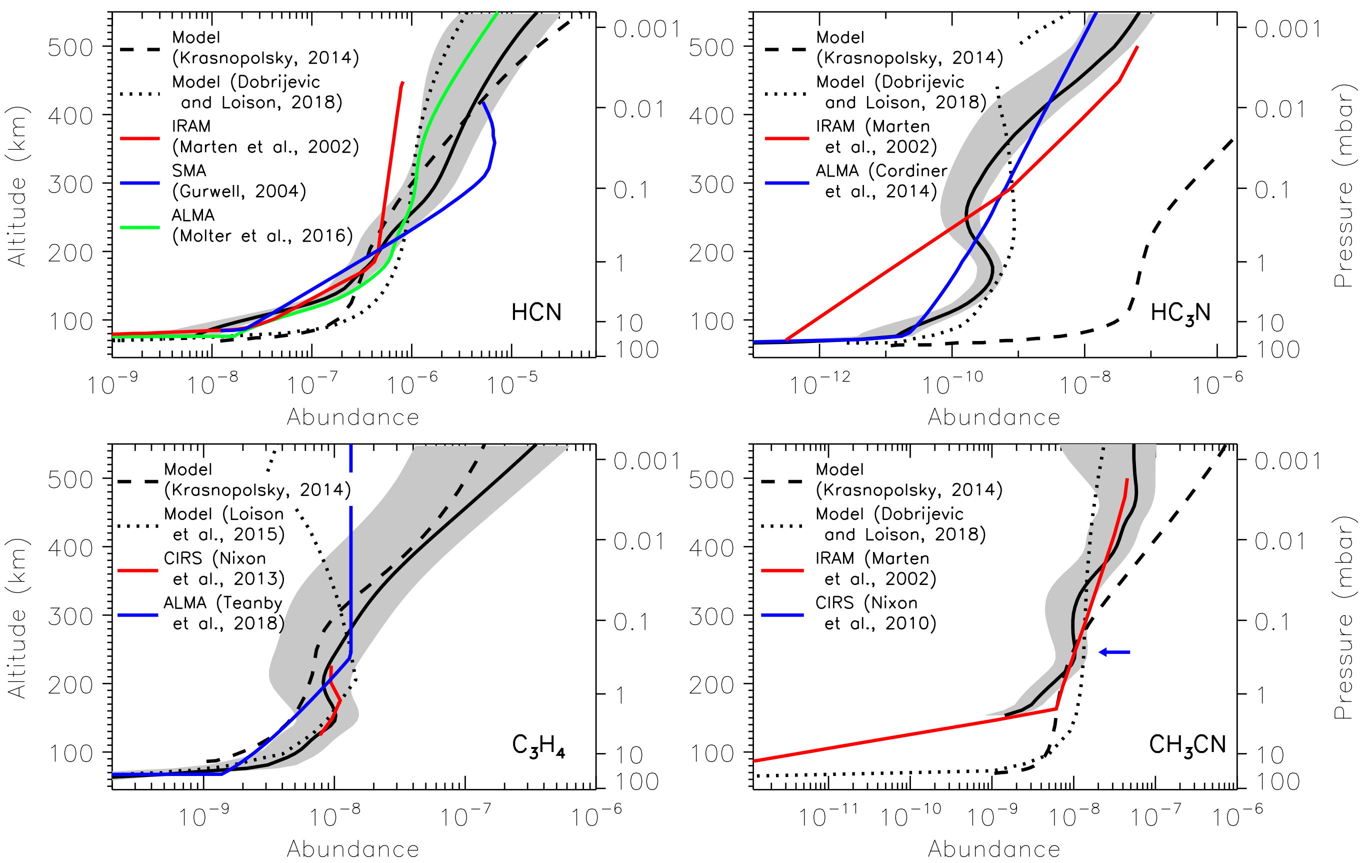

Figure 14: Comparisons of our mean, disk-averaged abundance profiles (solid black lines) and the retrieval errors (gray envelopes) for each molecule (see Fig. 10) to: photochemical models (black dashed and dotted lines), including Krasnopolsky (2014), Loison et al. (2015), and Dobrijevic and Loison (2018); and retrieved profiles from various ground and space-based observatories (colored lines) – including IRAM, the SMA, ALMA, and the *Cassini* orbiter – from Marten et al. (2002), Gurwell (2004), Nixon et al. (2010), Nixon et al. (2013), Cordiner et al. (2014), and Molter et al. (2016).

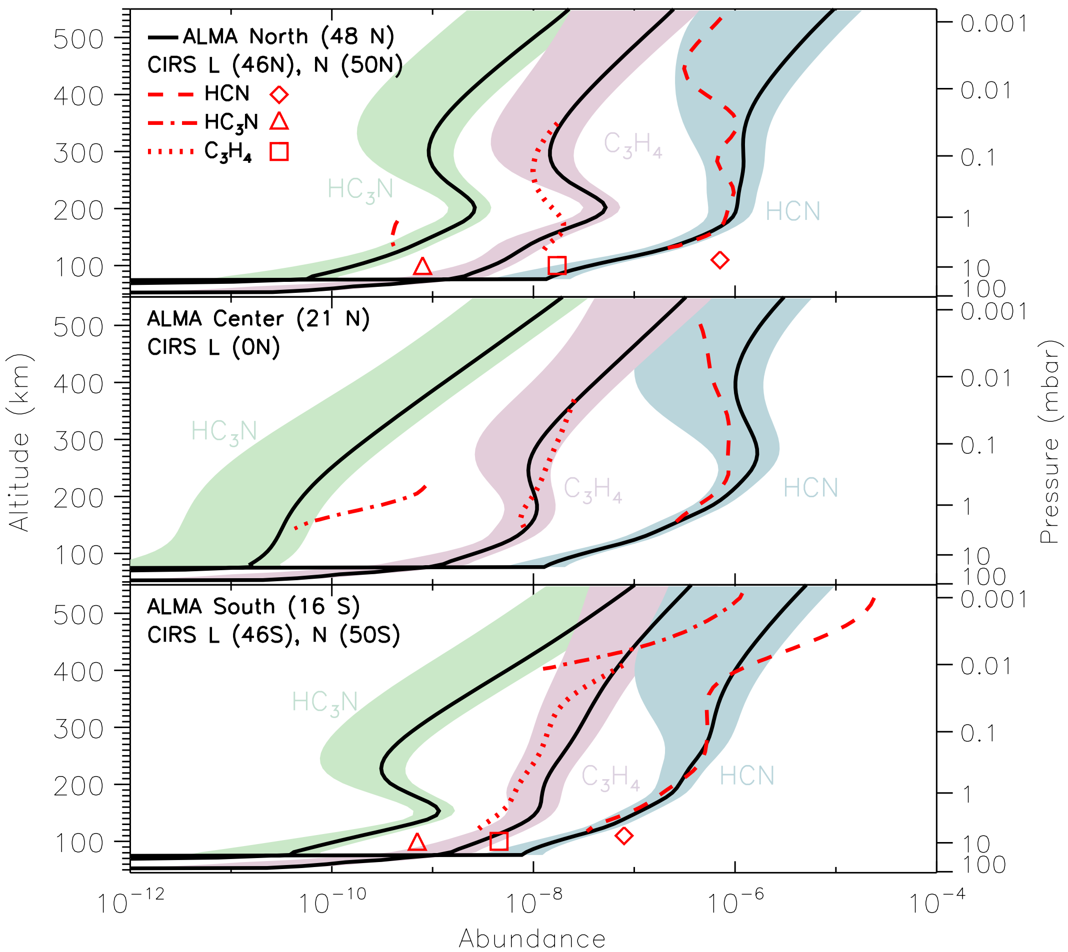

Figure 15: Comparisons of HCN, HC_3N profiles from Fig. 11 and C_3H_4 from Fig. 12 to *Cassini*/CIRS limb (L; red lines) measurements from Vinatier et al. (2015) and nadir (N; red symbols) from measurements by Coustenis et al. (2016) at comparable latitudes.

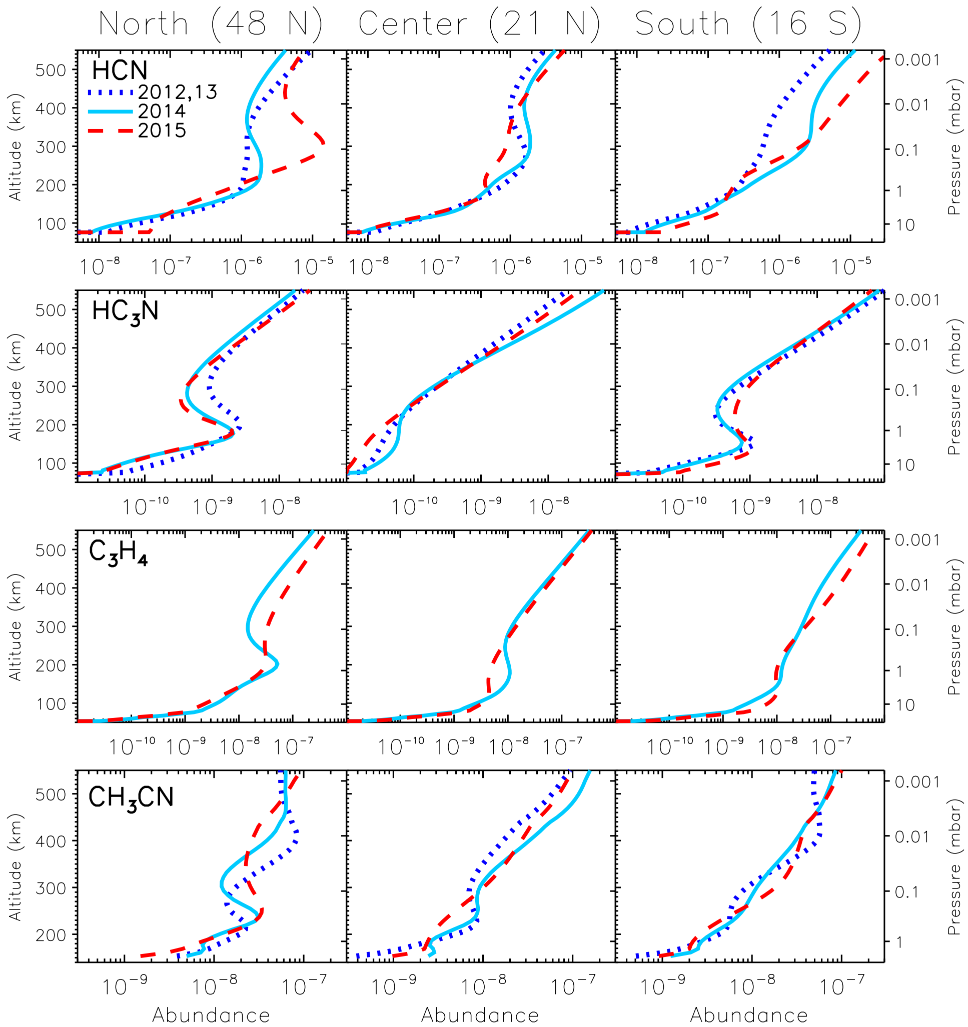

Figure 16: Temporal comparisons of abundance retrievals by species and region. North profiles in the first column; Center and South in the second and third columns. 2012 and 2013 retrievals are shown as blue dotted lines; 2014 profiles are shown in solid teal lines; 2015 retrievals are shown as dashed red lines.